Drosophila epidermal cells are intrinsically mechanosensitive and modulate nociceptive behavioral outputs

Jiro Yoshino[1,2,3*], Sonali S. Mali[3,4,5*], Claire R. Williams[1,3*], Takeshi Morita[3,6], Chloe E. Emerson[3], Christopher J. Arp[3], Sophie E. Miller[3], Chang Yin[1], Lydia Thé[4], Chikayo Hemmi[2], Mana Motoyoshi[2], Kenichi Ishii[2], Kazuo Emoto[2,7#], Diana M. Bautista[3,4,5#], and Jay Z. Parrish[1,3#]

[1]Department of Biology, University of Washington, Campus Box 351800, Seattle, WA 98195, USA

[2]Department of Biological Sciences, Graduate School of Science, The University of Tokyo, 7-3-1 Hongo, Bunkyo-ku, Tokyo 113-0033 Japan

[3]Division of Education, Marine Biological Laboratory, 7 MBL Street, Woods Hole, MA 02543, USA

[4]Department of Molecular and Cell Biology, University of California, Berkeley, CA 94720, USA

[5]Helen Wills Neuroscience Institute, University of California, Berkeley, CA 94720, USA

[6]Laboratory of Neurogenetics and Behavior, The Rockefeller University, 1230 York Avenue, New York, NY 10065

[7]International Research Center for Neurointelligence (WPI-IRCN), The University of Tokyo, 7-3-1 Hongo, Bunkyo-ku, Tokyo 113-0033 Japan

*These authors contributed equally to this work

[#]Correspondence: jzp2@uw.edu (lead contact), dbautista@berkeley.edu, or emoto@bs.s.u-tokyo.ac.jp

Abstract

Somatosensory neurons (SSNs) that detect and transduce mechanical, thermal, and chemical stimuli densely innervate an animal's skin. However, although epidermal cells provide the first point of contact for sensory stimuli. our understanding of roles that epidermal cells play in SSN function, particularly nociception, remains limited. Here, we show that stimulating *Drosophila* epidermal cells elicits activation of SSNs including nociceptors and triggers a variety of behavior outputs, including avoidance and escape. Further, we find that epidermal cells are intrinsically mechanosensitive and that epidermal mechanically evoked calcium responses require the store-operated calcium channel Orai. Epidermal cell stimulation augments larval responses to acute nociceptive stimuli and promotes prolonged hypersensitivity to subsequent mechanical stimuli. Hence, epidermal cells are key determinants of nociceptive sensitivity and sensitization, acting as primary sensors of noxious stimuli that tune nociceptor output and drive protective behaviors.

Introduction

The ability to detect tissue-damaging noxious stimuli and mount an escape response is essential for survival. Likewise, prolonged hypersensitivity following injury is an important form of plasticity that protects an animal from further damage. In *Drosophila*, a single class of identified somatosensory neurons (SSNs), class IV dendrite arborization (C4da) neurons, are necessary and sufficient for nociception; inactivating C4da neurons renders larvae insensitive to noxious stimuli whereas activating these neurons drives nocifensive behavior responses (Hwang *et al.*, 2007; Hu *et al.*, 2017; Burgos *et al.*, 2018). A variety of agents that cause tissue damage including UV irradiation and chemical toxins induce long-lasting allodynia and hyperalgesia (Babcock *et al.*, 2009; Boiko *et al.*, 2017), but this damage-induced hypersensitivity develops on a timescale of hours. *Drosophila* also display acute hypersensitivity noxious mechanical stimuli (Hu *et al.*, 2017). However, the cellular and molecular mechanisms underlying mechanical pain hypersensitivity remain enigmatic.

Recent studies demonstrate that epidermal cells work in concert with SSNs to transduce noxious and innocuous physical stimuli. For example, epidermal Merkel cells are mechanosensory cells that signal to sensory neurons to mediate touch transduction (Maksimovic *et al.*, 2014; Hoffman *et al.*, 2018). Similarly, keratinocytes are directly activated by noxious thermal and mechanical stimuli and release molecules that modulate nociceptor functions (Chung *et al.*, 2004; Koizumi *et al.*, 2004; Moqrich *et al.*, 2005; Mandadi *et al.*, 2009; Liu *et al.*, 2019; Sadler *et al.*, 2020). Furthermore, epidermal cells in invertebrates and vertebrates ensheathe nociceptors in mesaxon-like structures (Cauna, 1973; Chalfie and Sulston, 1981; Han *et al.*, 2012; Kim *et al.*, 2012a; O'Brien *et al.*, 2012; Jiang *et al.*, 2019), and these sheaths may serve as sites of epidermis-nociceptor signaling (Yin *et al.*, 2021). Indeed, epidermal ensheathment is required for normal responses to noxious mechanical stimuli in *Drosophila* (Jiang *et al.*, 2019). However, whether epidermal cells are directly activated by noxious stimuli and modulate C4da neuronal activity has not been studied.

Here, we examined the capacity of *Drosophila* epidermal cells to drive nociceptor activation and modulate mechanical nociceptive responses. We found that stimulation of epidermal cells, but no other non-neuronal cell types in the larval body wall evokes

activity in a variety of SSNs neurons and triggers nocifensive behavioral responses. Our *in vitro* and *ex vivo* calcium imaging experiments demonstrate that epidermal cells are intrinsically mechanosensitive. Using an unbiased genetic screen, we discovered a role for the store-operated calcium channel Orai, and its activator Stim in epidermal mechanotransduction and mechanical sensitization. Downstream of Stim/Orai activation, epidermal cells evoke nociceptor activation and mechanical hypersensitivity via epidermal vesicular release. Overall, we demonstrate that *Drosophila* epidermis-neuron signaling mediates both the acute detection of noxious mechanical stimuli and a form of prolonged mechanical hypersensitivity.

Results

Stimulation of epidermal cells evokes nocifensive behavior

To identify peripheral non-neuronal cell types that contribute to nociception, we conducted an optogenetic screen for light-evoked nocifensive behavior. First, as a benchmark for comparison we used the light-activated cation channel CsChrimson (Klapoetke *et al.*, 2014) to optogenetically activate nociceptive C4da neurons. Consistent with prior reports (Hwang *et al.*, 2007; Hu *et al.*, 2017), C4da activation triggered nocifensive behaviors including c-bending and rolling in 100% of larvae (Fig. 1A, Fig. 1S1A, Movie S1). Next, we selectively expressed CsChrimson using GAL4 drivers in combination with *elav-GAL80*, which effectively silences GAL4 expression in larval sensory neurons (Fig. 1S2), to target the six principle non-neuronal cell types within the larval body wall: epidermis, trachea, muscle, hemocytes, oenocytes, and glia (Fig. 1S3, Key Resources Table). We then monitored light-evoked behavioral outputs associated with stimulation of each cell type. We found that optogenetic stimulation of epidermal cells, like C4da neurons, elicited nocifensive c-bending and/or rolling behaviors in 73% of larvae (Fig. 1A, 1S1B), without significantly altering nociceptor morphogenesis (Fig. 1S4). In contrast, stimulation of other body wall cell types elicited a variety of non-nociceptive behavior outputs: for example, muscle stimulation triggered hunching behavior followed by prolonged freezing, whereas glia stimulation reproducibly induced only hunching behavior (Fig. 1S1C-I) (Zimmermann *et al.*, 2009). Thus,

epidermal cells are the only non-neuronal body wall cell type that triggers robust nocifensive behavioral responses.

To further validate the selective ability of body wall epidermal cells to drive nocifensive behaviors, we examined eight other epidermal drivers in addition to *R38F11-GAL4*, which displays no expression in sensory neurons and limited non-epidermal cell expression overall (Fig. 1S5). We found that optogenetic stimulation evoked nocifensive behaviors with each of the eight epidermal driver lines we tested: seven of the lines displayed rolling behavior while all eight displayed c-bending (Fig. 1B, Fig. 1S6). Although the previously described pan-epidermal *A58-GAL4* driver (Galko and Krasnow, 2004) drove robust nocifensive rolling responses (Fig. 1B, 1S6), *A58-GAL4* is expressed broadly in the larval CNS (Fig. 1S7) and stochastically expressed in sensory neurons (Jiang et al 2014). In contrast, the remaining seven drivers including *R38F11-GAL4* exhibited limited expression aside from epidermal cells, with no detectable expression in nociceptors, other larval SSNs, or peripheral glia, and highly restricted or undetectable expression in the CNS (Fig. 1S7). Further underscoring the connection between epidermal stimulation and nocifensive responses, the nocifensive behavioral response with these epidermal drivers correlated with the proportion of epidermal expression (Fig 1B).

We next used thermogenetic stimulation with the warmth-activated TRP channel dTRPA1 (Hamada *et al.*, 2008) as an independent method of probing nociceptive responses triggered by epidermal cell activation. On its own, the thermal stimulus (35° C) rarely induced rolling behavior in control larvae bearing *UAS-TRPA1* alone. In contrast, we found that >75% of larvae expressing TRPA1 in all nociceptors exhibited rolling behavior in response to a thermal stimulus (Fig. 1C). Likewise, thermogenetic activation of epidermal cells induced robust rolling responses in >75% of larvae, and addition of GAL80 transgenes (*tsh-GAL80 elav-GAL80*) that silenced the sparse *R38F11-GAL4* VNC expression (Fig. 1S5) had no effect on the rolling frequency (Fig. 1C, Fig. 1S3). Altogether, these results demonstrate that epidermal stimulation evokes nocifensive responses in *Drosophila*. Of note, prior studies demonstrated that sparse thermogenetic activation of nociceptors (<5 cells) yielded no significant increase in nocifensive rolling whereas activation of >10 cells was required to elicit rolling

responses in a majority of larvae (Robertson *et al.*, 2013). Hence, epidermal stimulation likely engages numerous C4da neurons to elicit these behavioral responses.

In addition to C4da nociceptors, the epidermis is innervated by a variety of other SSNs including mechanosensory C3da and chordotonal (Cho) neurons and proprioceptive C1da neurons. Whereas direct stimulation of C4da nociceptors principally elicited nocifensive behavioral outputs, epidermal stimulation elicited an array of behaviors in addition to nocifensive responses, including freezing and hunching (Fig. 2A, 2B, Fig. 2 video 1 and 2), behaviors associated with stimulation of C3da and Cho neurons (Zhang *et al.*, 2013; Turner *et al.*, 2016). These data suggest that epidermal cells may broadly modulate SSN activity in *Drosophila*.

To examine whether different epidermis-evoked behaviors were associated with activation of distinct classes of SSNs, we compared epidermis-evoked and SSN-evoked behaviors. Stimulation of C4da, C3da and Cho neurons elicited distinct behavioral motifs: only C4da neurons elicited rolling behavior; stimulation of C3da and Cho neurons together elicited hunching, C-bending, and backing; stimulation of Cho neurons alone principally elicited hunching and freezing responses (Fig. 2A-2C, 2F). In contrast, optogenetic epidermal stimulation elicited all of these behaviors, with nocifensive behaviors (c-bending, rolling) predominating initially, followed by non-nociceptive behaviors (backing, freezing) (Fig. 2D, 2F, 2S1). We note that neither the behavioral motifs induced by epidermal or SSN stimulation nor the behavioral sequence induced by epidermal stimulation was recapitulated in effector-only controls (*UAS-CsChrimson* ATR+; Fig. 2S1E), demonstrating that the observed responses were driven by activation of the respective cell types.

We observed three striking differences in behavior evoked by stimulation of epidermal cells versus individual SSNs. First, although rapid, latency to rolling was significantly longer following epidermal stimulation compared to stimulation of C4da (Fig. 2F). Second, the duration of rolling, bending, and backing responses was significantly longer for epidermis versus SSN stimulation (Fig. 2G). Third, backing and freezing behaviors persisted beyond the duration of the light stimulus for epidermis but not SSN stimulation (Fig. 2H). In summary, we find that epidermal stimulation triggers

more robust, varied and prolonged behaviors compared to responses from direct stimulation of discrete SSN subtypes.

Somatosensory neurons are activated by epidermal stimulation

We next asked whether epidermal stimulation activates larval SSNs including C4da, C3da, C1da, and Cho neurons. To test this possibility, we developed a semi-intact larval preparation in which we optogenetically stimulated epidermal cells while simultaneously monitoring calcium responses in axon terminals of SSNs (Fig. 3A). We found that epidermal stimulation triggered rapid and robust calcium transients in nociceptive C4da neurons, responses that were not observed in the absence of ATR or in effector-only controls (Fig. 3B). Epidermal stimulation likewise evoked calcium transients in mechanosensory C3da and Cho neurons, and in proprioceptive C1da neurons (Fig. 3C-3E, 3S1). Hence, epidermal stimulation can broadly modulate activity of larval SSNs.

We next tested the requirement for SSN synaptic transmission in epidermis-evoked behaviors. We stimulated epidermal cells with CsChrimson while blocking SSN neurotransmitter release using tetanus toxin light chain (TnT) (Sweeney *et al.*, 1995). We found that inhibiting C4da or C3da + Cho neurotransmission significantly reduced the frequency and duration of epidermal-evoked rolling and backing behaviors, respectively (Fig. 3F, 3G, 3S2). These data suggest that C4da and C3da/Cho neurons act downstream of epidermal cells to drive behaviors. We note that TnT expression in C4da neurons did not completely block epidermis-evoked nocifensive behaviors, and this likely reflects both incomplete C4da neuron silencing and epidermal activation of other SSNs that promote nociceptive outputs including C3da neurons, C2da neurons, and Cho neurons (Ohyama *et al.*, 2015; Hu *et al.*, 2017; Burgos *et al.*, 2018). Further, silencing C4da or C3da/Cho neurons while stimulating epidermal cells led to an increase in the non-nocifensive behaviors hunching and freezing (Fig. 3F, 3G). These results, along with the observation that rolling behaviors predominate the early behavioral responses to epidermal stimulation (Fig. 2B), suggest that the nervous system prioritizes nocifensive behavioral outputs following epidermal stimulation. These data support a model in which epidermal cells and SSNs are functionally coupled.

Epidermal stimulation potentiates nociceptive neurons and behaviors

What is the physiological relevance of this functional coupling of epidermal cells and SSNs? To address this question, we compared calcium responses in C4da neurons to either simultaneous epidermal and C4da stimulation or C4da stimulation alone. Simultaneous stimulation significantly enhanced the magnitude and duration of calcium responses in C4da axons (Fig. 4A-4D, 4S1). Based on this prolonged calcium response, we hypothesized that simultaneous epidermis and C4da neuron stimulation would yield enhanced nocifensive behavior output. To test this, we optogenetically stimulated C4da neurons and epidermal cells individually or in combination using low intensity CsChrimson activation and monitored larval behavior responses. In this stimulation paradigm, simultaneous epidermal cell and C4da neuron stimulation resulted in rolling in 100% of larvae whereas selective stimulation of C4da neurons or epidermal cells induced rolling in only 63% or 18% of larvae, respectively (Fig. 4E, 4F). Furthermore, simultaneous stimulation elicited a significantly higher number of rolls among responders than stimulation of nociceptors or epidermal cells alone (26.9 rolls for C4da + Epi, 4.9 for C4da, and 5.3 for Epi stimulation; Fig 4G, 4H). Likewise, simultaneous stimulation significantly reduced the latency to the first roll (Fig. 4I) and increased the duration of rolling behaviors (Fig. 4J). We next tested whether this functional coupling extends to mechanical stimuli. We simultaneously presented larvae with a noxious mechanical stimulus and a low intensity optogenetic epidermal stimulus that was insufficient to trigger rolling on its own (0% response rate, n = 200). This concurrent epidermal stimulation significantly increased touch-evoked nocifensive responses, yielding a 91% or 49% increase in rolling responses to 20 mN or 50 mN Von Frey stimulus, respectively (Fig. 4K). We next probed the kinetics of this epidermis-induced mechanical sensitization.

When *Drosophila* larvae are presented with two nociceptive mechanical stimuli in succession, they exhibit enhanced behavioral responses to the second stimulus (Hu *et al.*, 2017). We hypothesized that selective epidermal stimulation would sensitize larvae to subsequent nociceptive mechanical stimuli. To test this hypothesis, larvae expressing the warmth-activated calcium-permeable channel dTRPA1 in epidermal cells were presented with a thermal stimulus, 32º C to activate dTRPA1, followed by a 40 mN

mechanical stimulus 10 s later (Fig. 4L). Indeed, we found that dTRPA1-mediated epidermal stimulation significantly sensitized larvae to a subsequent mechanical stimulus, increasing the roll probability more than two-fold. In contrast, dTRPA1-mediated stimulation of C4da neurons did not induce mechanical sensitization, and we confirmed this result with two independent C4da neuron drivers (Fig. 4L). Thus, activation of epidermal cells but not C4da nociceptors alone induces prolonged sensitization to noxious mechanical stimuli. We next assessed the duration of sensitization following transient epidermal activation. Thermogenetic epidermal stimulation yielded persistent sensitization that recovered over a timescale of minutes (τ = 337 sec, Fig. 4M, 4N). The magnitude and duration of mechanical sensitization by thermogenetic epidermal stimulation was remarkably similar to sensitization evoked by a prior mechanical stimulus (63% roll probability in response to a second stimulus, τ = 334 sec, Fig. 4N, 4S1B). Altogether our data support a model whereby epidermal cells are mechanosensitive cells that signal to SSNs to drive acute nocifensive behaviors and prolong mechanical sensitization.

Epidermal cells are intrinsically mechanosensitive

Prior studies have shown that vertebrate epidermal cells directly respond to mechanical stimuli (Koizumi *et al.*, 2004; Haeberle *et al.*, 2008; Tsutsumi *et al.*, 2009; Ranade *et al.*, 2014; Woo *et al.*, 2014; Moehring *et al.*, 2018). Therefore, we next assessed whether *Drosophila* epidermal cells are intrinsically mechanosensitive. We developed a protocol to acutely dissociate epidermal cells and measure the responses of individual GCaMP6s-expressing epidermal cells to mechanical stimuli (Fig. 5A). We found that radial stretch elicits calcium responses in epidermal cells in a dose-dependent manner. For example, a low 0.5% stretch activated 18% of cells and a subsequent 1% stretch recruited an additional 10% of stretch-responding cells (Fig. 5B-5D). Overall, 51% of epidermal cells displayed stretch sensitivity (Fig. 5C, 5D). We also found that 43% of epidermal cells responded to hypoosmotic challenge and 35% responded to laminar flow; 19% of epidermal cells responded to both hypoosmotic challenge and laminar flow (Fig. 5S1). Given that dissociated epidermal cells were intrinsically mechanosensitive, we next assessed mechanically evoked responses in a semi-intact body wall

preparation (Fig. 5E). We found that 50% of epidermal cells exhibited a robust calcium transient in response to a 25 µm membrane displacement using a glass probe (Fig. 5E-5G, 5S1G). Altogether, these results indicate that *Drosophila* larval epidermal cells are intrinsically mechanosensitive.

Mechanically evoked epidermal responses rely on store-operated calcium entry

Our studies demonstrate that, like vertebrate keratinocytes, *Drosophila* epidermal cells exhibit mechanically evoked calcium transients. What is the mechanism of mechanotransduction in these cells? RNA-seq analysis of acutely dissociated epidermal cells revealed expression of more than 20 cation channels, including the mechanosensitive ion channels Piezo, TMEM63, and TMCO (Fig. 6S1). We assessed the epidermal requirements of these channels in mechanical nociception using available RNAi transgenes (Fig. 6A). Our behavioral screen identified one channel, *Orai*, the sole *Drosophila* pore-forming subunit of the Ca^{2+} release-activated Ca^{2+} (CRAC) channel (Feske *et al.*, 2006), that blocked mechanically-evoked nociceptive sensitization without impacting behavioral responses to the first stimulus (Fig. 6A, 6B, 6S2A) or altering nociceptor morphogenesis (Fig. 1S4). Interestingly, our screen uncovered an epidermal role for *Task6*, an orthologue of stretch-sensitive 2-pore potassium channels (Fink *et al.*, 1996), in mechanonociception, as *Task6* RNAi increased nocifensive rolling responses to the initial mechanical stimulus (Fig. 6S2B). Finally, although our RNAi studies did not reveal an epidermal requirement for other known mechanosensitive cation channels in mechanonociceptive behaviors, it is possible that multiple channels function redundantly, or that RNAi knockdown was incomplete.

To gain insight into mechanically evoked nociceptive sensitization, we focused on probing the role of Orai in epidermal mechanosensory responses. We first asked whether Orai is functional in *Drosophila* epidermal cells. Orai is a store-operated calcium (SOC) channel that is activated by the calcium-sensitive, endoplasmic reticulum (ER) molecule Stim, upon calcium release from ER calcium stores. Thapsigargin (TG) induces calcium release from intracellular stores and thus triggers Stim-dependent activation of Orai channels. Indeed, *Drosophila* epidermal cells displayed TG-induced calcium release from stores in the absence of extracellular calcium, followed by calcium

influx upon re-addition of extracellular calcium (Fig. 6C). Calcium influx was significantly inhibited by the addition of low nanomolar lanthanum, consistent with the high sensitivity of Orai channels to lanthanides (Fig. 6S2C). This characteristic store operated calcium entry (SOCE) response was significantly reduced by epidermis-specific *Stim* or *Orai* RNAi knockdown (Fig. 6S2D-6S2F). Consistent with a key role for SOCE in mechanotransduction, we found that radial stretch in the absence of extracellular calcium induced calcium release from intracellular stores, as well as calcium influx upon re-addition of extracellular calcium. These data show that mechanically evoked responses in epidermal cells involve both ER calcium release and store-operated calcium entry. While both store release and calcium influx constitute the calcium response to stretch, in 69% of cells, calcium due to store release exceeded that of calcium re-entry (Fig. 6E). Consistent with this observation, depletion of intracellular stores and inhibition of calcium influx reduced the number of stretch sensitve cells by 61% (stretch non-responsive cells in WT = 49% vs. store depleted = 80%) and 30% (stretch non-responsive cells in WT = 49% vs. La^{3+} = 64%; Fig. 6F-G), respectively. Given that Stim and Orai mediate SOCE, we investigated requirements for epidermal Stim and Orai in mechanically evoked calcium responses. RNAi knockdown of either *Stim* or *Orai* significantly reduced the fraction of stretch-responsive epidermal cells (RNAi control = 48%, *Stim* RNAi = 22%, *Orai* RNAi = 24%; Fig. 6H-I), with *Stim* or *Orai* RNAi preferentially attenuating stretch evoked responses to larger magnitude stretch stimuli. We also found that human keratinocytes display dose-dependent stretch evoked calcium responses, though they respond to higher magnitudes of stretch than *Drosophila* epidermal cells (Fig. 6J). Like Drosophila epidermal cells, both ER calcium release and store-operated calcium entry constitute the mechanically-evoked calcium responses in human keratinocytes (Fig. 6K).

Two hallmarks of Orai channels are steep inward rectification, with larger currents at hyperpolarizing potentials, and highly cooperative Orai activation by Stim (Hoover and Lewis, 2011). Since Stim and Orai mediate mechanical responses of epidermal cells *in vitro*, we predicted that increasing the calcium driving force through Orai activity by either hyperpolarizing *Drosophila* epidermal cells or by activating additional Orai channels via *Stim* overexpression would enhance behavioral responses

to mechanical stimuli. Indeed, we found that hyperpolarizing epidermal cells with the light-activated anion channelrhodopsin GtACR1 (Mohammad *et al.*, 2017) increased behavioral responses to mechanical stimuli (Fig. 6L). In addition, overexpressing *Stim* in epidermal cells significantly enhanced nocifensive behavioral responses to mechanical stimuli (Fig. 6M). Altogether, these results demonstrate that mechanically evoked responses of epidermal cells and the resulting nocifensive behavior outputs require store-operated calcium entry.

How might mechanically evoked calcium entry in epidermal cells drive nociceptor activation and behavior? Stim/Orai-mediated calcium entry contributes to exocytosis in a variety of cell types, including neurons and immune cells (Pores-Fernando and Zweifach, 2009; Ashmole *et al.*, 2012; Maneshi *et al.*, 2020; Chanaday *et al.*, 2021; Ramesh *et al.*, 2021). Therefore, we investigated the contribution of epidermal exocytosis in nociceptive sensitization with the temperature-sensitive dynamin mutant *shibire*^{ts} (*shi*^{ts}) to inducibly block vesicle recycling, as this treatment rapidly and potently blocks neurotransmitter release (Koenig *et al.*, 1983) and we found that acute epidermal dynamin inactivation using *UAS-shi*^{ts} had no discernable effect on nociceptor morphogenesis (Fig. 1S4). In this paradigm, larvae expressing *shi*^{ts} in epidermal cells, but not control larvae, exhibited significant attenuation of mechanically evoked nociceptive sensitization following pre-incubation at the non-permissive temperature (Fig. 6N). In contrast, both genotypes exhibited comparable responses to a mechanical stimulus at the permissive temperature (25° C) and to the first mechanical stimulus following pre-incubation at the non-permissive temperature (30° C). Taken together, these results are consistent with a model in which mechanical stimuli induce calcium influx and vesicular release from epidermal cells, which in turn activates nociceptors to induce acute nocifensive behaviors and prolonged sensitization (Fig. 6O). Although our RNA-seq analysis of epidermal cells did not reveal expression of neurotransmitter biosynthesis genes, epidermal cells express a large repertoire of genes involved in vesicular release as well as several neuropeptide genes, providing an entry point to defining the molecules involved in epidermis-SSN communication (Fig. 6S3).

Discussion

In this study, we have shown an essential role for *Drosophila* epidermal cells in escape responses to noxious mechanical stimuli. Activation of epidermal cells acutely activates SSNs to induce an array of behavioral outputs and mechanical sensitization. This epidermal potentiation persists for minutes to promote a prolonged, but reversible, mechanical hypersensitivity that may protect from further insult. This is distinct from previously described forms of neuropathic thermal and mechanical hypersensitivity in *Drosophila* which are induced by tissue damage and chemotherapeutic agents, respectively, emerge on a timescale of hours, and are long-lasting (Babcock *et al.*, 2009; Boiko *et al.*, 2017; Khuong *et al.*, 2019). In the mammalian somatosensory system, a variety of inflammatory mediators have been shown to activate TRPA1 in neurons to promote mechanical hypersensitivity (Bautista *et al.*, 2006); however, the molecular force transducers that mediate mechanical pain are unknown. In contrast, in the *Drosophila* somatosensory system, *Ppk1*/*Ppk26*, *Piezo*, and *Trpa1* are key transducers of mechanonociception (Zhong *et al.*, 2010; Kim *et al.*, 2012b; Gorczyca *et al.*, 2014; Guo *et al.*, 2014; Mauthner *et al.*, 2014). Prolonged sensitization to noxious mechanical stimuli plays an important protective role in an organism's survival; yet the mechanisms of mechanical sensitization of *Drosophila* nociceptors were unknown.

We demonstrate a new role for SOC signaling in both *Drosophila* and human epidermal cell mechanotransduction. While short-term sensitization is beneficial to survival, a key hallmark of pathological pain is prolonged and persistent mechanical hypersensitivity; whether deregulation of this mechanism of epidermis-evoked short-term sensitization contributes to pathological pain remains to be determined. Overall, we identified a mechanism that does not impact acute nociception but selectively regulates mechanical sensitization. These findings highlight Stim/Orai signaling as a new avenue for understanding mechanical pain.

This work has opened several new directions for future studies. First, how does radial and osmotic stretch lead to the activation of store-operated calcium signaling? Although Orai has not previously been shown to be mechanosensitive, our studies revealed a requirement for Orai and its activator Stim in mechanically-evoked calcium flux in *Drosophila* epidermal cells. We also showed that radial stretch of human keratinocytes triggered both calcium release from stores and SOCE; our previous

studies showed that Stim and Orai are required for SOCE in human keratinocytes (Wilson *et al.*, 2013). These data, in combination with other studies showing that mechanical stimulation of human mesenchymal stem cells and mouse enteroendocrine cells (Knutsen et al., 2023; (Kim *et al.*, 2015; Knutson *et al.*, 2023) also triggers SOCE suggests that Stim/Orai signaling may represent a conserved pathway for mechanotransduction in non-neuronal cells.

Second, how is Stim/Orai function linked to mechanotransduction? Stim/Orai signaling is activated downstream of G-protein coupled receptors (GPCRs) and receptor tyrosine kinases (RTKs) through phospholipase C. Studies have shown that a number GPCRs are mechanosensitive (Chachisvilis *et al.*, 2006; Grosmaitre *et al.*, 2007; Mederos y Schnitzler *et al.*, 2008; Connelly *et al.*, 2015; Xu *et al.*, 2018). Indeed, this mechanism has been proposed for mechanically evoked enteroendocrine activation in the gut epithelium (Knutson *et al.*, 2023), though this has not been studied in epidermal cells. Alternatively, plasma membrane deformation has been shown to induce formation of ER-plasma membrane junctions (Venturini *et al.*, 2020; Aoki *et al.*, 2021), where Stim and Orai clusters accumulate and interact to drive calcium influx (Luik *et al.*, 2008). Finally, a recent paper demonstrated that mechanical stimulation of the ER membrane itself promotes calcium release from ER stores via the opening of calcium-permeable ion channels in the ER membrane (Song *et al.*, 2024).

Third, how does mechanically induced signaling in epidermal cells lead to modulation of SSNs? Our data support a model whereby epidermal cells and multiple classes of SSNs are functionally coupled. Epidermal stimulation modulates activity of nociceptive C4da neurons, mechanosensory C3da and Cho neurons, and proprioceptive C1da neurons, and the output of neuronal activity is required for epidermis-evoked behaviors. We demonstrated a requirement for dynamin-dependent vesicle release from epidermal cells in mechanical sensitization, providing a potential link between Stim/Orai signaling in epidermal cells and downstream neuronal activity. However, the mediators that are released by epidermal cells and the signaling molecules in the nociceptors remain unknown. Furthermore, whether different types of SSNs are coupled to epidermal cells by distinct mechanisms remains to be determined. At least in the case of Cho neurons which are wrapped by ensheathing glial cells and

scolopale cells, signaling from epidermal cells likely involves at least one additional cell type. Finally, we find that epidermal cells exhibit a dose-dependent response to radial stretch; we therefore anticipate that the output of epidermal cells is likewise dependent on the stimulus intensity. Hence, rather than a fixed threshold beyond which epidermal cells are selectively activated, we hypothesize that increasing stimulus intensities drive increasing signal outputs to neurons.

Epidermal cells ensheathe peripheral arbors of some SSNs, including *Drosophila* nociceptive C4da neurons and, to a lesser extent, mechanosensory C3da neurons (Jiang *et al.*, 2019). Hence, epidermal sheaths could facilitate transduction of epidermal signals that modulate nociceptor function. Consistent with this possibility, blocking ensheathment attenuates *Drosophila* larval responses to noxious mechanical stimuli (Jiang *et al.*, 2019) and likewise impairs function of some *C. elegans* mechanosensory neurons (Chen and Chalfie, 2014). However, our finding that epidermal stimulation evokes calcium responses from SSNs that are not ensheathed by epidermal cells (C1da, Cho neurons) argues that epidermal sheaths are unlikely to play an essential function in epidermis-SSN functional coupling. Instead, ensheathment may facilitate nociceptor activation by increasing the efficiency of vesicular exchange or, alternatively, may modulate nociceptor activity through enhanced ionic coupling to epidermal cells.

Which epidermal-derived molecules might modulate neuronal activity? There are several mechanisms by which mammalian epidermal cells activate SSNs. Vesicular release of norepinephrine from mouse epidermal Merkel cells is required for sustained touch-evoked firing of mechanosensory neurons (Hoffman *et al.*, 2018). Additionally, mechanical stimuli trigger ATP release from mouse keratinocytes that activates nociceptors via purinergic (P2X4) receptors (Koizumi *et al.*, 2004; Tsutsumi *et al.*, 2009; Moehring *et al.*, 2018). Finally, Stim/Orai-dependent SOCE mediates the release of the cytokine thymic stromal lymphopoietin (TSLP) from epidermal keratinocytes that directly activates a subset of TRPA1-expressing SSNs to induce itch (Wilson *et al.*, 2013). Similar to these mammalian models, UV-damage has been shown to induce the release of the cytokine Eiger to promote *Drosophila* nociceptor sensitization (Babcock *et al.*, 2009); though this occurred on a slower timescale than the epidermal-evoked mechanical sensitization we describe here (8 h vs. ~ 10 sec, Fig. 4L). Likewise,

epidermal platelet-derived growth factor (PDGF) ligands regulate mechanonociceptive responses in *Drosophila* (Lopez-Bellido *et al.*, 2019) and intrathecal delivery of PDGF or the closely related growth factor EGFR yields mechanical hypersensitivity in rats (Masuda *et al.*, 2009; Puig *et al.*, 2020), but it remains to be determined whether growth factor signaling can yield rapid sensitization. Hence, future studies will address which neurotransmitters, neuropeptides, or inflammatory mediators underlie epidermal cell-mediated mechanical sensitization.

Our data support a model whereby epidermal cells and multiple classes of SSNs are functionally coupled. Future studies will address which neurotransmitters, neuropeptides, or inflammatory mediators underlie epidermal cell-mediated mechanical sensitization. An additional key next step is understanding whether the neuronal plasticity underlying mechanical sensitization results from the direct modulation of mechanosensitive channels or rapid insertion of new mechanosensitive channels into the plasma membrane, or from changes in the signaling pathways or channels that regulate neuronal excitability. Overall, we performed an unbiased genetic screen that for the first time establishes a key role for mechanically evoked Stim/Orai calcium signaling in epidermal cells that drive nociceptor modulation and mechanical hypersensitivity.

Material and Methods

Materials availability and community standards

Raw sequencing reads and gene expression estimates are available in the NCBI Sequence Read Archive (SRA) and in the Gene Expression Omnibus (GEO) under accession number GSE284380. Raw data used for analyses in this study is presented in the supplementary materials as Source Data and details of statistical analyses are presented in Supplementary File 1. ICMJE guidelines were used to define authorship roles and the ARRIVE essential 10 guidelines were used for the reporting of our in vivo studies.

Drosophila strains

Flies were maintained on standard cornmeal-molasses-agar media and reared at 25° C under 12 h alternating light-dark cycles. For all experiments involving optogenetic

manipulations, larvae were raised in the constant dark at 25 °C on Nutri-Fly Instant Food (Genesee Scientific #66-117), supplemented with 1 mM all-trans retinal (ATR; Sigma #R2500). A complete list of alleles used in this study is provided in the Key Resources Table. Experimental genotypes are listed in figure legends.

Cell lines

A human keratinocyte cell line (HaCaT) was used in this study. HaCaT cells were obtained from Cytion (Sioux Falls, SD), who performed STR authentication and mycoplasma-free certification.

Behavior analysis

Optogenetic behavior screen

Individual larvae were rinsed in ddH2O, transferred to an agarose substrate (1% agarose, 100 mm dish) in a darkened arena, and habituated for 30 s. Larvae were stimulated with a top-mounted 488 nM LED illuminator (PE-300, CoolLED) and images were captured with a sCMOS camera (Orca Flash 3.0, Hamamatsu) at frame acquisition rate of 20 fps and behaviors were scored before, during and after optogenetic stimulation.

High resolution video tracking of optogenetic-gated larval behavior

Following 5 min of light deprivation including 15 s of habituation in the behavioral arena, larvae were tracked before, during and after optical stimulus (10 s each, 30 s total) (Fig. 2A). For these studies we modified our stimulation paradigm in two key ways: to avoid potential contributions of nociceptor light evoked responses (Xiang *et al.*, 2010), we stimulated larvae using yellow-shifted light; and to facilitate kinetic analysis of behavior outputs, we used an automated shutter. Larvae were stimulated with a top-mounted 585 nm LED illuminator (SPECTRA X, Lumencor) equipped with a filter (FF01 585/40-25, Semrock), and images were captured with a sCMOS camera (Zyla4.2, Andor) at a frame rate of 20Hz. Larvae were constantly illuminated with an infrared (940 nm) light source (LDR2-132IR2-940-LA, CSS) for visualization. Larvae were fed (ATR+) or vehicle alone (ATR-) as indicated. Illumination intensities for optogenetic behavior

studies were: 300 μW/mm^2 for Fig. 1S6, Fig. 2B-2E, Fig. 2S1, Fig. 3E-3F, Fig. 3S2A-3S2C; 25 μW/mm^2 for Fig. 4E-4J; 1.16 μW/mm^2 for Fig. 4K. Annotated videos showing responses of representative larvae to optogenetic epidermal and nociceptor stimulation are provided in Figure 2 – movie 1 and 2.

Thermogenetic behavior assays

Larvae for thermogenetic assays were reared at room temperature (20° C) to limit TRPA1 activation during development. Third instar larvae were isolated from their food, washed in distilled water, and recovered to damp agar plates for several min, and transferred individually to a Peltier plate held at 25° C or 35° C. Behavior responses were recorded under infrared light with a computer-controlled GigE camera (FLIR) at an acquisition rate of 20 fps for 20 s. Responses were analyzed post-hoc blind to genotype and were plotted as the proportion of larvae that exhibited at least one complete nocifensive roll during stimulus application.

Mechanonociception assays

Third instar larvae were isolated from their food, washed in distilled water, and placed on a scored 35 mm petri dish with a thin film of water such that larvae stayed moist but did not float. Larvae were stimulated dorsally between segments A4 and A7 with calibrated Von Frey filaments that delivered the indicated force upon buckling, and nocifensive rolling responses were scored during the 10 s following stimulus removal. For assays involving multiple stimuli, larvae were stimulated individually, allowed to freely locomote in the arena for up to 1 min (for longer recoveries larvae were recovered onto 2% agar to prevent desiccation), and subsequently presented with the second stimulus. For assays involving thermal and mechanical stimuli, larvae were individually transferred to a pre-warmed Peltier plate containing a thin layer of water, incubated for the indicated time, and transferred to the behavior arena (or a 2% agar plate for recoveries > 1 min) with a paint brush for subsequent mechanical stimulation. For assays involving optical and mechanical stimuli, larvae were raised in constant dark at 25 °C on food supplemented with 1 mM all-trans retinal (detailed above), transferred to the behavior arena with 25 μW/mm^2 broad spectrum illumination, and assayed for

responses to mechanical stimuli. All assays were conducted in ambient light except for experiments with GtACR (Fig. S72), which were conducted under 500-700 nm LED illumination (CoolLED PE-300, green). Our illumination setup for these experiments provided limited working distance, therefore larvae were restrained with forceps and given only a single stimulus.

Video annotations

Videos of individual larvae responding to light stimuli were scored on a frame-by-frame basis using the annotation software BORIS (Friard and Gamba, 2016). Behaviors scored, along with descriptions of the criteria for each behavior, are detailed in Table S1. Video analysts were blind to the genotype and treatment during scoring. Scoring on a training set was compared across all analysts to calibrate, and any behaviors for which the primary analyst was uncertain were reviewed by an additional analyst. Additionally, 10% of videos were scored independently by two analysts and there was at least 80% concordance in behaviors annotated in these comparisons.

Microscopy

Calcium imaging: ventral nerve cords

Third-instar larvae were dissected along the dorsal midline and pinned on a sylgard-coated dish (Sylgard 184, Dow Corning). The internal organs except for neural tissues were removed. Larvae were bathed in HL3.1 (Feng et al, 2004) modified to remove calcium (Table S2) to minimize larval movement. The ventral nerve cord was imaged using an Olympus BX51WI microscope, equipped with a spinning-disk confocal unit Yokogawa CSU10 (Yokogawa) and an EM-CCD digital camera (Evolve, Photometrics). For activation of epidermal cells with the light gated CsChrimson, red light was delivered by a pE-300 (CoolLED) equipped with a filter (ET645/30x, Chroma) at a light intensity of 30 $\mu W/mm^2$. Obtained images were analyzed using Metamorph (https://www.moleculardevices.com/systems/metamorph-research-imaging) and ImageJ (Schneider *et al.*, 2012). Baseline fluorescence was calculated as the mean fluorescence intensity of an ROI over the ten frames prior to light stimulus delivery. The trapezoidal method was used to calculate area under the curve, utilizing the trapz

function of MATLAB. Data points from the onset of stimulation to the end of stimulation were used for the calculation.

Calcium imaging: fillet preparations

Third-instar larvae were dissected along the ventral midline and pinned on sylgard (Dow Corning) dishes with the internal surface facing towards the microscope. All internal organs, including the central nervous system, were removed. Larvae were bathed in calcium-containing HL3.1 (Feng *et al.*, 2004) (Table S2) except where indicated and images of the dorsal midline between abdominal segments A2 and A4 were captured with a Zeiss Axio Zoom V16 microscope. Captured images were analyzed using ç (Schneider *et al.*, 2012). Mechanical stimulus: fillets were poked with a tapered borosilicate capillary with a rounded tip, using a micromanipulator to induce a deflection of 25 µm. The decay time constant was calculated by fitting the data points from the peak response to the end of the experiment into an exponential curve f(x) = a*exp(b*x) using MATLAB with R^2>0.9 used as a threshold for reliable fitting.

Calcium imaging: dissociated epidermal cells

Six to eight larval fillets were dissociated in 400 µL of 50% Saline (modified Ringer's recipe) / 50% Schneider's media with 200 U/mL collagenase type I (Fisher 17-100-017), with mixing at 1000 RPM at 33°C for 16 min, with trituration every 8 min. Undigested fillets were removed and the remaining suspension was spun at 500 g for 3 min, followed by aspiration of the supernatant down to a 10 µL cell suspension. Cells were resuspended in 30 µL fresh PBS / Schneider's solution and plated onto poly-D-lysine (1 mg/ml, Sigma P7886) coated No. 1 coverslips, with 10 µL cell solution per coverslip. Cells were cultured at least 30 min and up to 2 h at 25° C prior to imaging. Cells were imaged using a 10x objective at a frame rate of 0.33 Hz. Solutions are indicated in figure legends (see Table S2 for recipes). Obtained images were analyzed using MetaFluor and Python and baseline fluorescence was calculated as the mean fluorescence intensity of an ROI over 5 frames prior to stimulus delivery. For stretch stimulation, circular membranes were cut with an arch punch from sheets of glossy silicone of 0.01–0.02 inch thickness (Specialty Manufacturing, Inc.) and coated with 1

mg/ml poly-D-lysine for 1 h before plating cells. Membranes were mounted onto the StageFlexer system and vacuum pressure was applied through the FX-3000 system (Flexcell). Calibrations were performed using fluorescent beads attached to the membranes, and images were taken before and during a static stretch. To stimulate cells, a 2 s square wave of vacuum pressure was applied. Cells were imaged with an Olympus BX61WI upright microscope. For store-operated calcium entry measurements and osmotic stimulation, cells were imaged using a Zeiss Observer inverted microscope and solutions were perfused using the Automate Scientific ValveLink 8.2 perfusion system. At the end of each imaging session, 1uM ionomycin was perfused and only cells that showed a calcium response, as defined by a 10% increase from baseline fluorescence, were used in analysis. Flow, osmotic and radial stretch responders were defined by a 5% increase from baseline fluorescence.

Calcium imaging: human keratinocytes

Immortalized human keratinocytes (HaCaT) cells (Cytion) were plated on silicone membranes one day prior to stretch experiments. Prior to the radial stretch experiments, cells were loaded with 1 μm Fura-2AM supplemented with 0.01% Pluronic F-127 (w/v, Life Technologies) in a physiological Ringer's solution containing the following (in mm): 140 NaCl, 5 KCl, 10 HEPES, 2 CaCl2, 2 MgCl2, and 10 d-(+)-glucose, pH 7.4. Acquired images were displayed as the ratio of 340 nm/380 nm. Cells that had a response 10 standard deviations above baseline to ionomycin were included in the analysis and stretch responses were defined by a 15% increase in Fura-2 340/380 ratio.

Confocal Microscopy

For peripheral imaging of cellular morphology, live single larvae were mounted in 90% glycerol under a coverslip and imaged on a Leica SP5 confocal microscope using a 40x 1.25 NA lens. To image the larval CNS, larvae were dissected on sylgard plates, briefly fixed in 4% paraformaldehyde (PFA) in PBS for 15 min at room temperature, washed 3 x 5 min in PBS, and mounted for imaging.

RNA-Seq analysis of epidermal cells

RNA isolation for RNA-Seq

Larvae with cytoplasmic GFP expressed in different epidermal subsets were microdissected and dissociated in collagenase type I (Fisher 17-100-017) into single cell suspensions, largely as previously described (Williams *et al.*, 2016), with the addition of 1% BSA to the dissociation mix. After dissociation, cells were transferred to a new 35 mm petri dish with 1 mL 50% Schneider's media, 50% PBS supplemented with 1% BSA. Under a fluorescent stereoscope, individual fluorescent cells were manually aspirated with a glass pipette into PBS with 0.5% BSA, and then serially transferred until isolated without any additional cellular debris present. Ten cells per sample were aspirated together, transferred to a mini-well containing 3ul lysis solution (0.2 % Triton X-100 in water with 2 U / µL RNAse Inhibitor), lysed by pipetting up and down several times, transferred to a microtube, and stored at -80º C. For the picked cells, 2.3 µL of lysis solution was used as input for library preparation.

RNA-Seq library preparation

RNA-Seq libraries were prepared from the picked cells following the Smart-Seq2 protocol for full length transcriptomes (Picelli *et al.*, 2014). To minimize batch effects, primers, enzymes, and buffers were all used from the same lots for all libraries. Libraries were multiplexed, pooled, and purified using AMPure XP beads, quality was checked on an Agilent TapeStation, and libraries were sequenced as 51-bp single end reads on a HiSeq4000 at the UCSF Center for Advanced Technology.

RNA-Seq data analysis

Reads were demultiplexed with CASAVA (Illumina) and read quality was assessed using FastQC (https://www.bioinformatics.babraham.ac.uk/) and MultiQC (Ewels *et al.*, 2016). Reads containing adapters were removed using Cutadapt version 2.4 (Martin, 2011) and reads were mapped to the *D. melanogaster* transcriptome, FlyBase genome release 6.29, using Kallisto version 0.46.0 (Bray *et al.*, 2016) with default parameters. AA samples were removed from further analysis for poor quality, including low read depth (< 500,000 reads), and low mapping rates (< 80%). Raw sequencing reads and

gene expression estimates are available in the NCBI Sequence Read Archive (SRA) and in the Gene Expression Omnibus (GEO) under accession number GSE284380.

Statistical analysis

For each experimental assay control populations were sampled to estimate appropriate sample numbers to allow detection of ~33% differences in means with 80% power over a 95% confidence interval. Details of statistical tests including treatment groups, sample numbers (which correspond to independent biological replicates), statistical tests, p-values and q-values are provided in Supplementary File 1.

Acknowledgements

This work was supported by grants from the National Institutes of Health to JZP (NINDS R01 NS076614; NINDS R21NS125795), DMB (NICHD K99 HD086271), CRW (5F31NS106775), and the MBL (R25NS063307); a grant from the National Science Foundation to SSM (NSF GRFP DGE1752814); funding from the Leading Initiative for Excellent Young Researchers (LEADER) from MEXT, JSPS (KAKENHI 22K06309), and AMED-PRIME (JP22gm6510011) to KI; a grant from the Weill Neurohub to JZP and DMB; a grant from the Scan Design Foundation, a JSPS long-term fellowship and startup funds from UW (J.Z.P); MEXT Grants-in-Aid for Scientific Research (KAKENHI 16H06456), JSPS (KAKENHI 16H02504), WPI-IRCN, AMED-CREST (JP22gm310010), and JST-CREST to KE; and a fellowship from the Grass Foundation (CEE). DMB. is an HHMI investigator. Fly Stocks obtained from the Bloomington *Drosophila* Stock Center (NIH P40OD018537) were used in this study. We thank Jessica Huang, Jordan Martel, and David Shen for assistance with video tracking; Peter Soba for helpful discussions.

Author Contributions

Conception and design: Optogenetic behavior analysis, K.E., J.Z.P, C.R.W, J.Y.; larval behavior assays, J.Z.P, C.R.W, and J.Y.; in vivo calcium imaging, K.E., J.Z.P, C.R.W, J.Y.; ex vivo calcium imaging, D.M.B., S.S.M., and J.Z.P

Acquisition of data: Optogenetic behavior screen, C.J.A, C.E.E., S.M., and J.Y.; Optogenetic behavior assays, J.Y., C.H., M.M., K.I., and C.R.W.; mechanonociception

assays, C.R.W, and J.Z.P; thermogenetic behavior assays, J.Z.P.; RNA-sequencing, J.Z.P. and C.R.W.

Analysis and Interpretation of data: larval behavior assays, J.Z.P, C.R.W, J.Y.; in vivo calcium imaging, K.E., J.Z.P, C.R.W, J.Y.; ex vivo calcium imaging, D.M.B. and S.S.M.; transcriptomic data, C.H., C.R.W., and J.Z.P.

Drafting the article: D.M.B., J.Z.P, C.R.W, S.S.M., and J.Y.

Competing Interests

DMB is on the scientific advisory board of Escient Pharmaceuticals. The remaining authors declare no conflicts of interest.

References

Aoki, K, Harada, S, Kawaji, K, Matsuzawa, K, Uchida, S, and Ikenouchi, J (2021). STIM-Orai1 signaling regulates fluidity of cytoplasm during membrane blebbing. Nat Commun 12, 480.

Ashmole, I, Duffy, SM, Leyland, ML, Morrison, VS, Begg, M, and Bradding, P (2012). CRACM/Orai ion channel expression and function in human lung mast cells. J Allergy Clin Immunol 129, 1628-1635.e2.

Babcock, DT, Landry, C, and Galko, MJ (2009). Cytokine signaling mediates UV-induced nociceptive sensitization in Drosophila larvae. Curr Biol 19, 799–806.

Bautista, DM, Jordt, S-E, Nikai, T, Tsuruda, PR, Read, AJ, Poblete, J, Yamoah, EN, Basbaum, AI, and Julius, D (2006). TRPA1 mediates the inflammatory actions of environmental irritants and proalgesic agents. Cell 124, 1269–1282.

Boiko, N, Medrano, G, Montano, E, Jiang, N, Williams, CR, Madungwe, NB, Bopassa, JC, Kim, CC, Parrish, JZ, Hargreaves, KM, *et al.* (2017). TrpA1 activation in peripheral sensory neurons underlies the ionic basis of pain hypersensitivity in response to vinca alkaloids. PLoS ONE 12, e0186888.

Bray, NL, Pimentel, H, Melsted, P, and Pachter, L (2016). Near-optimal probabilistic RNA-seq quantification. Nat Biotechnol 34, 525–527.

Burgos, A, Honjo, K, Ohyama, T, Qian, CS, Shin, GJ-E, Gohl, DM, Silies, M, Tracey, WD, Zlatic, M, Cardona, A, *et al.* (2018). Nociceptive interneurons control modular motor pathways to promote escape behavior in Drosophila. Elife 7.

Cauna, N (1973). The free penicillate nerve endings of the human hairy skin. J Anat 115, 277–288.

723 Chachisvilis, M, Zhang, Y-L, and Frangos, JA (2006). G protein-coupled receptors sense fluid
724 shear stress in endothelial cells. Proc Natl Acad Sci U S A 103, 15463–15468.

725 Chalfie, M, and Sulston, J (1981). Developmental genetics of the mechanosensory neurons of
726 Caenorhabditis elegans. Dev Biol 82, 358–370.

727 Chanaday, NL, Nosyreva, E, Shin, O-H, Zhang, H, Aklan, I, Atasoy, D, Bezprozvanny, I, and
728 Kavalali, ET (2021). Presynaptic store-operated Ca2+ entry drives excitatory spontaneous
729 neurotransmission and augments endoplasmic reticulum stress. Neuron 109, 1314-1332.e5.

730 Chen, X, and Chalfie, M (2014). Modulation of C. elegans touch sensitivity is integrated at
731 multiple levels. J Neurosci 34, 6522–6536.

732 Chung, M-K, Lee, H, Mizuno, A, Suzuki, M, and Caterina, MJ (2004). TRPV3 and TRPV4 mediate
733 warmth-evoked currents in primary mouse keratinocytes. J Biol Chem 279, 21569–21575.

734 Connelly, T, Yu, Y, Grosmaitre, X, Wang, J, Santarelli, LC, Savigner, A, Qiao, X, Wang, Z, Storm,
735 DR, and Ma, M (2015). G protein-coupled odorant receptors underlie mechanosensitivity in
736 mammalian olfactory sensory neurons. Proc Natl Acad Sci U S A 112, 590–595.

737 Ewels, P, Magnusson, M, Lundin, S, and Käller, M (2016). MultiQC: summarize analysis results
738 for multiple tools and samples in a single report. Bioinformatics 32, 3047–3048.

739 Feng, Y, Ueda, A, and Wu, C-F (2004). A modified minimal hemolymph-like solution, HL3.1, for
740 physiological recordings at the neuromuscular junctions of normal and mutant Drosophila
741 larvae. J Neurogenet 18, 377–402.

742 Feske, S, Gwack, Y, Prakriya, M, Srikanth, S, Puppel, S-H, Tanasa, B, Hogan, PG, Lewis, RS, Daly,
743 M, and Rao, A (2006). A mutation in Orai1 causes immune deficiency by abrogating CRAC
744 channel function. Nature 441, 179–185.

745 Fink, M, Duprat, F, Lesage, F, Reyes, R, Romey, G, Heurteaux, C, and Lazdunski, M (1996).
746 Cloning, functional expression and brain localization of a novel unconventional outward
747 rectifier K+ channel. EMBO J 15, 6854–6862.

748 Friard, O, and Gamba, M (2016). BORIS: a free, versatile open-source event-logging software for
749 video/audio coding and live observations. Methods in Ecology and Evolution 7, 1325–1330.

750 Galko, MJ, and Krasnow, MA (2004). Cellular and genetic analysis of wound healing in
751 Drosophila larvae. PLoS Biol 2, E239.

752 Gorczyca, DA, Younger, S, Meltzer, S, Kim, SE, Cheng, L, Song, W, Lee, HY, Jan, LY, and Jan, YN
753 (2014). Identification of Ppk26, a DEG/ENaC Channel Functioning with Ppk1 in a Mutually
754 Dependent Manner to Guide Locomotion Behavior in Drosophila. Cell Rep 9, 1446–1458.

Grosmaitre, X, Santarelli, LC, Tan, J, Luo, M, and Ma, M (2007). Dual functions of mammalian olfactory sensory neurons as odor detectors and mechanical sensors. Nat Neurosci 10, 348–354.

Guo, Y, Wang, Y, Wang, Q, and Wang, Z (2014). The role of PPK26 in Drosophila larval mechanical nociception. Cell Rep 9, 1183–1190.

Haeberle, H, Bryan, LA, Vadakkan, TJ, Dickinson, ME, and Lumpkin, EA (2008). Swelling-activated Ca2+ channels trigger Ca2+ signals in Merkel cells. PLoS One 3, e1750.

Hamada, FN, Rosenzweig, M, Kang, K, Pulver, SR, Ghezzi, A, Jegla, TJ, and Garrity, PA (2008). An internal thermal sensor controlling temperature preference in Drosophila. Nature 454, 217–220.

Han, C, Wang, D, Soba, P, Zhu, S, Lin, X, Jan, LY, and Jan, Y-N (2012). Integrins regulate repulsion-mediated dendritic patterning of drosophila sensory neurons by restricting dendrites in a 2D space. Neuron 73, 64–78.

Hoffman, BU, Baba, Y, Griffith, TN, Mosharov, EV, Woo, S-H, Roybal, DD, Karsenty, G, Patapoutian, A, Sulzer, D, and Lumpkin, EA (2018). Merkel Cells Activate Sensory Neural Pathways through Adrenergic Synapses. Neuron 100, 1401-1413.e6.

Hoover, PJ, and Lewis, RS (2011). Stoichiometric requirements for trapping and gating of Ca2+ release-activated Ca2+ (CRAC) channels by stromal interaction molecule 1 (STIM1). Proc Natl Acad Sci U S A 108, 13299–13304.

Hu, C, Petersen, M, Hoyer, N, Spitzweck, B, Tenedini, F, Wang, D, Gruschka, A, Burchardt, LS, Szpotowicz, E, Schweizer, M, *et al.* (2017). Sensory integration and neuromodulatory feedback facilitate Drosophila mechanonociceptive behavior. Nat Neurosci 20, 1085–1095.

Hwang, RY, Zhong, L, Xu, Y, Johnson, T, Zhang, F, Deisseroth, K, and Tracey, WD (2007). Nociceptive neurons protect Drosophila larvae from parasitoid wasps. Curr Biol 17, 2105–2116.

Jiang, N, Rasmussen, JP, Clanton, JA, Rosenberg, MF, Luedke, KP, Cronan, MR, Parker, ED, Kim, H-J, Vaughan, JC, Sagasti, A, *et al.* (2019). A conserved morphogenetic mechanism for epidermal ensheathment of nociceptive sensory neurites. Elife 8.

Jiang, N, Soba, P, Parker, E, Kim, CC, and Parrish, JZ (2014). The microRNA bantam regulates a developmental transition in epithelial cells that restricts sensory dendrite growth. Development 141, 2657–2668.

Khuong, TM, Wang, Q-P, Manion, J, Oyston, LJ, Lau, M-T, Towler, H, Lin, YQ, and Neely, GG (2019). Nerve injury drives a heightened state of vigilance and neuropathic sensitization in Drosophila. Sci Adv 5, eaaw4099.

Kim, ME, Shrestha, BR, Blazeski, R, Mason, CA, and Grueber, WB (2012a). Integrins establish dendrite-substrate relationships that promote dendritic self-avoidance and patterning in drosophila sensory neurons. Neuron 73, 79–91.

Kim, SE, Coste, B, Chadha, A, Cook, B, and Patapoutian, A (2012b). The role of Drosophila Piezo in mechanical nociception. Nature 483, 209–212.

Kim, T-J, Joo, C, Seong, J, Vafabakhsh, R, Botvinick, EL, Berns, MW, Palmer, AE, Wang, N, Ha, T, Jakobsson, E, *et al.* (2015). Distinct mechanisms regulating mechanical force-induced Ca^{2+} signals at the plasma membrane and the ER in human MSCs. Elife 4, e04876.

Klapoetke, NC, Murata, Y, Kim, SS, Pulver, SR, Birdsey-Benson, A, Cho, YK, Morimoto, TK, Chuong, AS, Carpenter, EJ, Tian, Z, *et al.* (2014). Independent optical excitation of distinct neural populations. Nature Methods 11, 338–346.

Knutson, KR, Whiteman, ST, Alcaino, C, Mercado-Perez, A, Finholm, I, Serlin, HK, Bellampalli, SS, Linden, DR, Farrugia, G, and Beyder, A (2023). Intestinal enteroendocrine cells rely on ryanodine and IP3 calcium store receptors for mechanotransduction. J Physiol 601, 287–305.

Koenig, JH, Saito, K, and Ikeda, K (1983). Reversible control of synaptic transmission in a single gene mutant of Drosophila melanogaster. J Cell Biol 96, 1517–1522.

Koizumi, S, Fujishita, K, Inoue, K, Shigemoto-Mogami, Y, Tsuda, M, and Inoue, K (2004). Ca2+ waves in keratinocytes are transmitted to sensory neurons: the involvement of extracellular ATP and P2Y2 receptor activation. Biochem J 380, 329–338.

Liu, X, Wang, H, Jiang, Y, Zheng, Q, Petrus, M, Zhang, M, Zheng, S, Schmedt, C, Dong, X, and Xiao, B (2019). STIM1 thermosensitivity defines the optimal preference temperature for warm sensation in mice. Cell Res 29, 95–109.

Lopez-Bellido, R, Puig, S, Huang, PJ, Tsai, C-R, Turner, HN, Galko, MJ, and Gutstein, HB (2019). Growth Factor Signaling Regulates Mechanical Nociception in Flies and Vertebrates. J Neurosci 39, 6012–6030.

Luik, RM, Wang, B, Prakriya, M, Wu, MM, and Lewis, RS (2008). Oligomerization of STIM1 couples ER calcium depletion to CRAC channel activation. Nature 454, 538–542.

Maksimovic, S, Nakatani, M, Baba, Y, Nelson, AM, Marshall, KL, Wellnitz, SA, Firozi, P, Woo, S-H, Ranade, S, Patapoutian, A, *et al.* (2014). Epidermal Merkel cells are mechanosensory cells that tune mammalian touch receptors. Nature 509, 617–621.

Mandadi, S, Sokabe, T, Shibasaki, K, Katanosaka, K, Mizuno, A, Moqrich, A, Patapoutian, A, Fukumi-Tominaga, T, Mizumura, K, and Tominaga, M (2009). TRPV3 in keratinocytes transmits temperature information to sensory neurons via ATP. Pflugers Arch 458, 1093–1102.

Maneshi, MM, Toth, AB, Ishii, T, Hori, K, Tsujikawa, S, Shum, AK, Shrestha, N, Yamashita, M, Miller, RJ, Radulovic, J, *et al.* (2020). Orai1 Channels Are Essential for Amplification of Glutamate-Evoked Ca2+ Signals in Dendritic Spines to Regulate Working and Associative Memory. Cell Rep 33, 108464.

Masuda, J, Tsuda, M, Tozaki-Saitoh, H, and Inoue, K (2009). Intrathecal delivery of PDGF produces tactile allodynia through its receptors in spinal microglia. Mol Pain 5, 23.

Mauthner, SE, Hwang, RY, Lewis, AH, Xiao, Q, Tsubouchi, A, Wang, Y, Honjo, K, Skene, JHP, Grandl, J, and Tracey, WD (2014). Balboa binds to pickpocket in vivo and is required for mechanical nociception in Drosophila larvae. Curr Biol 24, 2920–2925.

Mederos y Schnitzler, M, Storch, U, Meibers, S, Nurwakagari, P, Breit, A, Essin, K, Gollasch, M, and Gudermann, T (2008). Gq-coupled receptors as mechanosensors mediating myogenic vasoconstriction. EMBO J 27, 3092–3103.

Moehring, F, Cowie, AM, Menzel, AD, Weyer, AD, Grzybowski, M, Arzua, T, Geurts, AM, Palygin, O, and Stucky, CL (2018). Keratinocytes mediate innocuous and noxious touch via ATP-P2X4 signaling. Elife 7.

Mohammad, F, Stewart, JC, Ott, S, Chlebikova, K, Chua, JY, Koh, T-W, Ho, J, and Claridge-Chang, A (2017). Optogenetic inhibition of behavior with anion channelrhodopsins. Nat Methods 14, 271–274.

Moqrich, A, Hwang, SW, Earley, TJ, Petrus, MJ, Murray, AN, Spencer, KSR, Andahazy, M, Story, GM, and Patapoutian, A (2005). Impaired thermosensation in mice lacking TRPV3, a heat and camphor sensor in the skin. Science 307, 1468–1472.

Morin, X, Daneman, R, Zavortink, M, and Chia, W (2001). A protein trap strategy to detect GFP-tagged proteins expressed from their endogenous loci in Drosophila. Proc Natl Acad Sci USA 98, 15050–15055.

O'Brien, GS, Rieger, S, Wang, F, Smolen, GA, Gonzalez, RE, Buchanan, J, and Sagasti, A (2012). Coordinate development of skin cells and cutaneous sensory axons in zebrafish. J Comp Neurol 520, 816–831.

Ohyama, T, Schneider-Mizell, CM, Fetter, RD, Aleman, JV, Franconville, R, Rivera-Alba, M, Mensh, BD, Branson, KM, Simpson, JH, Truman, JW, *et al.* (2015). A multilevel multimodal circuit enhances action selection in Drosophila. Nature 520, 633–639.

Picelli, S, Faridani, OR, Björklund, AK, Winberg, G, Sagasser, S, and Sandberg, R (2014). Full-length RNA-seq from single cells using Smart-seq2. Nat Protoc 9, 171–181.

Pores-Fernando, AT, and Zweifach, A (2009). Calcium influx and signaling in cytotoxic T-lymphocyte lytic granule exocytosis. Immunol Rev 231, 160–173.

Puig, S, Donica, CL, and Gutstein, HB (2020). EGFR Signaling Causes Morphine Tolerance and Mechanical Sensitization in Rats. eNeuro 7, ENEURO.0460-18.2020.

Ramesh, G, Jarzembowski, L, Schwarz, Y, Poth, V, Konrad, M, Knapp, ML, Schwär, G, Lauer, AA, Grimm, MOW, Alansary, D, *et al.* (2021). A short isoform of STIM1 confers frequency-dependent synaptic enhancement. Cell Rep 34, 108844.

Ranade, SS, Woo, S-H, Dubin, AE, Moshourab, RA, Wetzel, C, Petrus, M, Mathur, J, Bégay, V, Coste, B, Mainquist, J, *et al.* (2014). Piezo2 is the major transducer of mechanical forces for touch sensation in mice. Nature 516, 121–125.

Robertson, JL, Tsubouchi, A, and Tracey, WD (2013). Larval defense against attack from parasitoid wasps requires nociceptive neurons. PLoS One 8, e78704.

Sadler, KE, Moehring, F, and Stucky, CL (2020). Keratinocytes contribute to normal cold and heat sensation. Elife 9, e58625.

Schneider, CA, Rasband, WS, and Eliceiri, KW (2012). NIH Image to ImageJ: 25 years of image analysis. Nat Methods 9, 671–675.

Song, Y, Zhao, Z, Xu, L, Huang, P, Gao, J, Li, J, Wang, X, Zhou, Y, Wang, J, Zhao, W, *et al.* (2024). Using an ER-specific optogenetic mechanostimulator to understand the mechanosensitivity of the endoplasmic reticulum. Dev Cell 59, 1396-1409.e5.

Sweeney, ST, Broadie, K, Keane, J, Niemann, H, and O'Kane, CJ (1995). Targeted expression of tetanus toxin light chain in Drosophila specifically eliminates synaptic transmission and causes behavioral defects. Neuron 14, 341–351.

Tsutsumi, M, Inoue, K, Denda, S, Ikeyama, K, Goto, M, and Denda, M (2009). Mechanical-stimulation-evoked calcium waves in proliferating and differentiated human keratinocytes. Cell Tissue Res 338, 99–106.

Turner, HN, Armengol, K, Patel, AA, Himmel, NJ, Sullivan, L, Iyer, SC, Bhattacharya, S, Iyer, EPR, Landry, C, Galko, MJ, *et al.* (2016). The TRP Channels Pkd2, NompC, and Trpm Act in Cold-Sensing Neurons to Mediate Unique Aversive Behaviors to Noxious Cold in Drosophila. Curr Biol 26, 3116–3128.

Venturini, V, Pezzano, F, Català Castro, F, Häkkinen, H-M, Jiménez-Delgado, S, Colomer-Rosell, M, Marro, M, Tolosa-Ramon, Q, Paz-López, S, Valverde, MA, *et al.* (2020). The nucleus measures shape changes for cellular proprioception to control dynamic cell behavior. Science 370, eaba2644.

Williams, CR, Baccarella, A, Parrish, JZ, and Kim, CC (2016). Trimming of sequence reads alters RNA-Seq gene expression estimates. BMC Bioinformatics 17, 103.

888 Wilson, SR, Thé, L, Batia, LM, Beattie, K, Katibah, GE, McClain, SP, Pellegrino, M, Estandian, DM,
889 and Bautista, DM (2013). The epithelial cell-derived atopic dermatitis cytokine TSLP activates
890 neurons to induce itch. Cell 155, 285–295.

891 Woo, S-H, Ranade, S, Weyer, AD, Dubin, AE, Baba, Y, Qiu, Z, Petrus, M, Miyamoto, T, Reddy, K,
892 Lumpkin, EA, *et al.* (2014). Piezo2 is required for Merkel-cell mechanotransduction. Nature 509,
893 622–626.

894 Xiang, Y, Yuan, Q, Vogt, N, Looger, LL, Jan, LY, and Jan, YN (2010). Light-avoidance-mediating
895 photoreceptors tile the Drosophila larval body wall. Nature 468, 921–926.

896 Xu, J, Mathur, J, Vessières, E, Hammack, S, Nonomura, K, Favre, J, Grimaud, L, Petrus, M,
897 Francisco, A, Li, J, *et al.* (2018). GPR68 Senses Flow and Is Essential for Vascular Physiology. Cell
898 173, 762-775.e16.

899 Yamamoto, M, Ueda, R, Takahashi, K, Saigo, K, and Uemura, T (2006). Control of axonal
900 sprouting and dendrite branching by the Nrg-Ank complex at the neuron-glia interface. Curr Biol
901 16, 1678–1683.

902 Yin, C, Peterman, E, Rasmussen, JP, and Parrish, JZ (2021). Transparent Touch: Insights From
903 Model Systems on Epidermal Control of Somatosensory Innervation. Front Cell Neurosci 15,
904 680345.

905 Zhang, W, Yan, Z, Jan, LY, and Jan, YN (2013). Sound response mediated by the TRP channels
906 NOMPC, NANCHUNG, and INACTIVE in chordotonal organs of Drosophila larvae. Proc Natl Acad
907 Sci USA 110, 13612–13617.

908 Zhong, L, Hwang, RY, and Tracey, WD (2010). Pickpocket is a DEG/ENaC protein required for
909 mechanical nociception in Drosophila larvae. Curr Biol 20, 429–434.

910 Zimmermann, G, Wang, L-P, Vaughan, AG, Manoli, DS, Zhang, F, Deisseroth, K, Baker, BS, and
911 Scott, MP (2009). Manipulation of an innate escape response in Drosophila: photoexcitation of
912 acj6 neurons induces the escape response. PLoS One 4, e5100.

913

914

Figure Legends

Figure 1. Stimulation of epidermal cells elicits nociceptive behaviors. (A) Fraction of larvae that exhibited optogenetic-induced rolling (roll probability) using the indicated GAL4 lines to drive *UAS-CsChrimson* expression. All experimental genotypes, except for larvae expressing *UAS-CsChrimson* in C4da neurons, included *elav-GAL80* to suppress neuronal GAL4 activity. Genotypes: *GAL4, UAS-CsChrimson, elav-GAL80/+*. (B) Roll probability of larvae following optogenetic stimulation using the indicated GAL4 lines in combination with *elav-GAL80* (or *tsh-GAL80* + *cha-GAL80* in the case of *A58-GAL4*) to drive *UAS-CsChrimson* expression in epidermal cells. All epidermal drivers except for *sr-GAL4*, which is expressed in apodemes but no other epidermal cells, elicited rolling responses. Genotypes: *GAL4, UAS-CsChrimson, elav-GAL80/+*. (C) Roll probability of larvae following thermogenetic stimulation using the indicated GAL4 line to express the warmth (35°C) -activated *UAS-TrpA1*. The number of rolling larvae (out of 50) is indicated for each group. Genotypes: *GAL4, UAS-TrpA1, GAL80 (as indicated)/+*. Control, *UAS-TrpA1/+*. Sample sizes are indicated in each panel. Asterisk (*) indicates $p<0.05$ in this and subsequent figures. Raw data for all figures is provided in Source Data File 1 and details of statistical analyses, including tests performed, p-values, and q-values are provided in Supplementary File 1.

Figure 1 – figure supplement 1. Related to Figure 1A. Detailed behavior analyses of larvae following optogenetic stimulation using the indicated GAL4 lines to express *UAS-CsChrimson*. (A-G) Behavior ethograms show behaviors of individual larvae (rows) prior to, during, and after application of the light stimulus (indicated by the blue bar above the ethogram). (H) Fraction of larvae exhibiting indicated behaviors and (I) duration of indicated behaviors during light stimulus.

Figure 1 – figure supplement 2. Related to Figure 1A. Efficacy of *GAL80* transgenes. Maximum intensity projections show body wall expression patterns of (A) the pan-da neuron driver $GAL4^{21\text{-}7}$ and (B) the nociceptor-specific driver *ppk-GAL4* with or without *elav-GAL80* to silence neuronal GAL4 expression. Note that *elav-GAL80* completely

suppresses GFP reporter expression from each of the drivers. Genotypes: (A) *GAL4$^{21-7}$ UAS-CD4-tdGFP/+* and *GAL4$^{21-7}$ UAS-CD4-tdGFP/+, elav-GAL80/+*, (B) *ppk-GAL4, UAS-CD4-tdGFP/+* and *ppk-GAL4, UAS-CD4-tdGFP/+, elav-GAL80/+*.

Figure 1 – figure supplement 3. Related to Figures 1A and 1C. Expression analysis of the pan-epidermal *R38F11-GAL4* driver. (A-B) Maximum intensity projections of confocal stacks show larval expression of a red fluorescent protein (*UAS-tdTomato*) under control of *R38F11-GAL4* in larvae additionally expressing *Nrg167-GFP*, an exon trap line that labels epidermal and glial membranes (Morin *et al.*, 2001; Yamamoto *et al.*, 2006). (A) Low-magnification view showing stereotyped expression in dorsal epidermis across multiple larval segments. Larvae are oriented dorsal-up. *R38F11-GAL4* is likewise expressed throughout the ventral and lateral epidermis. Compared to other epidermal drivers (see Fig. 1S5), *R38F11-GAL4* exhibited more uniform expression from segment to segment and among epidermal subpopulations within a given segment. (B) *R38F11-GAL4* expression in the dorsal epidermis of a single abdominal segment, A2. (C) High-resolution images of *R38F11-GAL4* expression visualized using a nuclear localized red fluorescent protein (*UAS-NLS-RFP*). Images depict expression in larval skin territory containing dorsal cluster of SSNs (visualized by HRP immunoreactivity), which includes the nociceptive neuron ddaC (outlined by dashed lines). Note that although *R38F11-GAL4* is expressed in epidermal cells, expression is undetectable in da neurons. The *R38F11-GAL4* expression domain likewise excludes SSNs throughout the body wall. (D) *R38F11-GAL4* expression of *UAS-NLS-RFP* in the larval CNS. *R38F11-GAL4* is expressed in a single motor neuron in each segment of the ventral ganglion, ~10 VNC interneurons, and <50 additional neurons in each brain hemisphere. (E-H) GAL80-mediated refinement of *R38F11-GAL4* expression. (E) *Tsh-GAL80* induced variegation in epidermal *R38F11-GAL4* expression and (F) suppressed VNC expression while expanding brain expression domains of *R38F11-GAL4*. (G) *Elav-GAL80* likewise induced epidermal variegation in *R38F11-GAL4* expression but (H) completely attenuated CNS expression. Dashed lines in (D, G, and H) outline the larval brain and ventral ganglion. Genotypes: (A-B) *Nrg^{G00305}/+; UAS-tdTomato/+; GAL4^{GMR38F11}/+*, (C) *GAL4^{GMR38F11}/+, UAS-NLS-RedStinger/+*, (E-F)

977 *Nrg^{G00305}/+; UAS-tdTomato/tsh-GAL80; GAL4^{GMR38F11}/+*, (G-H) *Nrg^{G00305}/+; UAS-NLS-*
978 *RedStinger/+; GAL4^{GMR38F11}/elav-GAL80*.
979
980 **Figure 1 – figure supplement 4**. Related to Figure 1A. Epidermal manipulations have
981 no effect on C4da neuron dendrite morphogenesis. (A) Maximum intensity projections
982 show dendrites of representative C4da neurons labeled with *ppk-CD4-tdGFP* in the
983 indicated treatment groups. (B) Morphometric analysis of C4da dendrites. Box plots
984 depict the total dendrite length (left) and the number of dendrite branchpoints (right)
985 normalized to larval segmental area in larvae containing the pan-epidermal driver
986 *R38F11-GAL4* and the indicated *UAS*-transgenes at 120 h AEL. Prior to imaging, *ppk-*
987 *CD4-tdGFP/+, R38F11-GAL4/UAS-shi^{TS}* larvae were incubated for 10 min at 30° C, as
988 in Fig. 6N. N $\geq$ 6 neurons for each genotype, points represent measurements from
989 individual neurons, boxes display the first and third quartiles, hatches mark medians,
990 and whiskers mark maximum and minimum values. ANOVA with post-hoc Tukey's test
991 revealed no significant difference between control and treatment groups for both
992 metrics. Genotypes: *ppk-CD4-tdGFP/+; R38F11-GAL4/+* without (-) or with a single
993 copy of the indicated *UAS*-transgenes.
994
995 **Figure 1 – figure supplement 5**. Related to Figures 1A and 1C. Expression patterns of
996 body wall *GAL4* drivers. Maximum intensity projections of tiled confocal stacks show
997 larval expression of membrane-targeted RFP (*UAS-mCD2-Cherry*) by the indicated
998 drivers in larvae additionally expressing the C4da neuron-specific marker *ppk-CD8-*
999 *GFP*. Scale bars, 500 µm. Genotypes: *ppk-mCD8-GFP/+; UAS-mCD2-Cherry/+;*
1000 *GAL4/+*
1001
1002 **Figure 1 – figure supplement 6**. Related to Figure 1B.
1003 (A-B) Behavior ethograms of larvae following pan-epidermal stimulation (denoted with a
1004 red bar) mediated by *A58-GAL4*. (C) Fraction of larvae exhibiting indicated behaviors
1005 and (I) duration of indicated behaviors during optogenetic stimulation. (Genotype: *A58-*
1006 *GAL4, UAS-CsChrimson, tsh-GAL80, cha-GAL80/+*). (E-K) Behavioral ethograms of
1007 larvae following optogenetic stimulation (denoted with a blue bar) with a panel of

epidermal GAL4 drivers. (L) Fraction of larvae exhibiting indicated behaviors and (M) duration of indicated behaviors during light stimulus. Genotype: *GAL4, UAS-CsChrimson, elav-GAL80/+*.

Figure 1 – figure supplement 7. Related to Figure 1B. Expression patterns of epidermal GAL4 drivers in the larval body wall and CNS. (A) Maximum intensity projections of confocal stacks show larval expression of a red fluorescent protein (*UAS-tdTomato*) under control of the indicated epidermal drivers in larvae additionally expressing *Nrg167-GFP*, an exon trap line that labels epidermal and glial membranes (Morin *et al.*, 2001; Yamamoto *et al.*, 2006). White brackets mark the location of the dorsal cluster of SSNs, which are visualized at high resolution in (B). (B) Maximum intensity projections of confocal stacks show larval expression of a nuclear-localized form of RFP (*UAS-RedStinger*) under control of the indicated *GAL4* drivers in larval fillets stained with fluorescently conjugated anti-HRP antibody to label sensory neurons. The nociceptive C4da neuron soma is outlined with a white hatched line in composite images and the outline is superimposed on images depicting *UAS-RedStinger* signal. Sensory neuron expression is undetectable for all epidermal drivers except for *A58-GAL4*, for which stochastic sensory neuron expression has been previously described (Jiang *et al.*, 2014). (C) Maximum intensity projections show CNS expression epidermal drivers used in this study. Aside from *A58-GAL4*, each driver exhibits sparse nervous system expression. Genotypes: (A) Nrg^{G00305}*/+; UAS-tdTomato/+; GAL4/+*, (B-C) *UAS-NLS-RFP/+; GAL4/+*.

Figure 2. Stimulation of epidermal cells evokes multimodal behavioral responses. (A) Larval behaviors were scored for 10 s before, during, and after optogenetic stimulation. (B-E) Fraction of larvae exhibiting indicated behaviors over time in one second bins expressing CsChrimson in (B) epidermal cells, (C) C4da neurons, (D) C3da neurons, and (E) Cho neurons in the presence and absence of all-trans retinal (ATR). Red line indicates the presence of light stimulation. (F) The latency to the first roll of the larvae that rolled from *Epi>Chrimson* ATR+ and *C4da>Chrimson* ATR+ treatment groups (n = 14, 17, respectively). (G) The duration of indicated behaviors of the larvae

that displayed those behaviors during optogenetic stimulation. (H) The fraction of larvae that exhibited indicated behaviors following removal of the light stimulus of all larvae from panels (B-E). Genotypes: *GAL4, UAS-CsChrimson*/+.

Figure 2 – video 1. Behavioral response of representative larva to optogenetic epidermal stimulation. Movies were captured under infrared light and annotated with behaviors that were scored post-hoc. Nociceptive behaviors (indicated in red) precede non-nociceptive behaviors (blue). Genotype: *R38F11-GAL4, UAS-CsChrimson*/+.

Figure 2 – video 2. Behavioral response of representative larva to optogenetic nociceptor stimulation. Genotype: *ppk-GAL4, UAS-CsChrimson*/+.

Figure 2 – figure supplement 1. (A-E) Behavior ethograms depict behaviors of individual larvae displayed in one second bins, scored for 10 s before, during, and after optical stimulus. Plots depict responses of larvae which contain a single copy of *UAS-CsChrimson* together with the indicated *GAL4* driver in the absence and presence of ATR (A-D), or responses of effector-only (*UAS-CsChrimson*/+, ATR+) controls (E). (F) Plot depicts the fraction of larvae exhibiting indicated behaviors during light stimulus. (G) Latency to the first bend, hunch, back and freeze behaviors following optogenetic stimulation. Genotypes: *GAL4, UAS-CsChrimson*/+.

Figure 3. (A) Optogenetic activation of CsChrimson-expressing epidermal cells in the body wall triggers calcium transients in the axon terminal of GCaMP6s-expressing nociceptive SSNs. Images show responses from one representative animal. Plots depict mean GCaMP6s fluorescence intensity of the axon terminals of (B) C4da, (C) C3da, (D) Cho, and (E) C1da neurons following optogenetic activation (light stimulus, yellow box) of epidermal cells over time. Solid lines depict mean GCaMP6s fluorescence across replicates (n=15 larval fillet preparations), shading indicates SEM, red traces are *GAL4*+ ATR+, blue traces are *GAL4*+ ATR-, black trace is *GAL4*- ATR+. (F) The fraction of larvae exhibiting indicated behaviors during optogenetic epidermal stimulation in combination with SSN silencing via Tetanus Toxin (TnT) expression. We note that

although baseline rolling probability is elevated in all genetic backgrounds containing the *AOP-LexA-TnT* insertion, silencing C4da and C3da neurons significantly attenuates responses to epidermal stimulation. (G) The duration of the behavioral responses during optogenetic epidermal stimulation with neuronal TnT expression. Genotypes: (A-B) *R27H06-LexA* (C4da neurons), *AOP-GCaMP6s, UAS-CsChrimson/+; R38F11-GAL4/+* or *R27H06-LexA* (C4da neurons), *AOP-GCaMP6s, UAS-CsChrimson/+* (*GAL4*-ATR-effector-only control); (C) *AOP-GCaMP6s, UAS-CsChrimson/+; R38F11-GAL4/NompC-LexA* (C3da neurons); (D) *UAS-GCaMP6s, AOP-CsChrimson, R61D08-GAL4* (Cho neurons)*/R38F11-LexA*; (E) *UAS-GCaMP6s, AOP-CsChrimson, R11F05-GAL4* (C1da neurons)*/R38F11-LexA*; (F-G) *R38F11-GAL4, UAS-CsChrimson, AOP-LexA-TnT/+* (*Epi>CsChrimson*); *R38F11-GAL4, UAS-CsChrimson, AOP-LexA-TnT/ppk-LexA* (*Epi>CsChrimson + C4da>TnT*); *R38F11-GAL4, UAS-CsChrimson, AOP-LexA-TnT/NompC-LexA* (*Epi>CsChrimson + C3da>TnT*).

Figure 3 – figure supplement 1. Related to Figure 3A-3D. GCaMP6s responses in axon terminals of (B) C4da, (C) C3da, (D) Cho and (E) C1da neurons following optogenetic activation (light stimulus, yellow box) of epidermal cells over time. Each trace represents the GCaMP6s fluorescence of an individual larval fillet. Red traces are *GAL4*+ ATR+, blue traces are *GAL4*+ ATR-, black trace is *GAL4*- ATR+. Genotypes: (A) *R27H06-LexA*, *AOP-GCaMP6s, UAS-CsChrimson/+; R38F11-GAL4/+* or *R27H06-LexA*, *AOP-GCaMP6s, UAS-CsChrimson/+* (*GAL4*-ATR- effector-only control); (B) *AOP-GCaMP6s, UAS-CsChrimson/+; R38F11-GAL4/NompC-LexA*; (C) *UAS-GCaMP6s, AOP-CsChrimson, R61D08-GAL4 /R38F11-LexA*; (D) *UAS-GCaMP6s, AOP-CsChrimson, R11F05-GAL4/R38F11-LexA*.

Figure 3 – figure supplement 2. Related to Figure 3E-3F. (A-C) Behavior ethograms (left) and fraction of larvae (right) exhibiting indicated behaviors to optogenetic epidermal stimulation in combination with (A) an *AOP-TNT* transgene (control lacking LexA driver), (B) C4da neuron silencing via Tetanus Toxin (TnT), and (C) C3da neuron silencing via TnT. (D) Fraction of larvae exhibiting each behavior and (E) the duration of

behavior responses after removal of the light stimulus. Genotypes are indicated in (A-C).

Figure 4. Epidermal stimulation augments nociceptive responses. (A) Mean GCaMP6s responses (F/F_0) in C4da axons during optogenetic stimulation (yellow box) of C4da neurons alone (green) or of C4da neurons and epidermal cells (magenta), shading indicates SEM. (B) Simultaneous epidermal stimulation increased the peak calcium response (F_{max}/F_0), (C) total calcium influx (area under the curve), and (D) duration of C4da neuron calcium responses compared to stimulation of C4da neurons alone. Genotypes: *ppk-LexA, AOP-GCAMP6s/+; R27H06-GAL4/UAS-CsChrimson* (C4da) and *ppk-LexA, AOP-GCAMP6s/+; R27H06-GAL4/R38F11-GAL4, UAS-CsChrimson* (C4da+epi). (E-J) Characterization of the behavioral responses to low-intensity optogenetic stimulation of C4da neurons, epidermal cells, or simultaneous C4da neurons and epidermal cells. (E) Cumulative and (F) total roll probability during optogenetic stimulation (indicated by the red bar). n = 33 (*C4da>CsChrimson*), 30 (*Epi>CsChrimson*), and 31 (*C4da + Epi>CsChrimson*) larvae. (G, H) Number and frequency distribution of rolls, (I) latency to the first roll observed for larvae of the indicated genotypes, and (J) the duration of the indicated behaviors during light stimulus. Genotypes: *UAS-CsChrimson/+; R27H06-GAL4/+* (C4da), *UAS-CsChrimson/+; R38F11-GAL4/+* (Epidermis), *UAS-CsChrimson/+; R27H06-GAL4/R38F11-GAL4* (C4da+Epidermis). (K) Roll probability of larvae to a 20 mN or 50 mN von Frey mechanical stimulus and epidermal optogenetic activation (a light stimulus, 1.16 $\mu W/mm^2$ that was insufficient on its own to induce nocifensive rolling). Larvae were reared in the presence or absence of ATR, as indicated. Genotypes: *UAS-CsChrimson/+; R38F11-GAL4/+*. (L-N) Prior epidermal but not nociceptor stimulus potentiates mechanical nociceptive responses. (L) Roll probability of control larvae (*UAS-TrpA1/+*) or larvae expressing TrpA1 in the epidermis (*Epi-GAL4: R38F11-GAL4)* or C4da neurons (*UAS-TrpA1/+*; *C4da-GAL4 #1: R27H06-GAL4, UAS-TrpA1/+*; *C4da-GAL4 #2: ppk-GAL4, UAS-TrpA1/+*), or control larvae (*no GAL4: UAS-TrpA1/+*;) in response to 40 mN mechanical stimulus 10 s following 10 s of a thermal stimulus (25º or 32º C). To control for effects of genetic background, we confirmed that each of the

experimental genotypes exhibited mechanically induced nociceptive sensitization (Fig. 4S1C). (M) Roll probability of control larvae (*UAS-TrpA1/+*) or larvae expressing TrpA1 in the epidermis (*Epi>TrpA1*: *R38F11-GAL4, UAS-TrpA1/+*) in response to a 40 mN mechanical stimulus delivered at the indicated time interval following a 32º C thermal stimulus. (N) Nociceptive enhancement (difference in the roll probablity to the first and second stimulus) is plotted against the recovery duration and results were fit to an exponential curve to derive the decay time constant. The red line indicates nociceptive enhancement of a mechanical stimulus by a prior epidermal thermogenetic stimulus; the black line indicates nociceptive enhancement by a prior mechanical stimulus.

Figure 4 – figure supplement 1. (A) GCaMP6s responses (F/F_0) of individual replicates during optogenetic stimulation (yellow box) of C4da neurons alone (green) or C4da neurons and epidermal cells (magenta), yellow box indicates presence of light stimulus. Genotypes: *ppk-LexA, AOP-GCAMP6s/+; R27H06-GAL4/UAS-CsChrimson* (C4da) and *ppk-LexA, AOP-GCAMP6s/+; R27H06-GAL4/R38F11-GAL4, UAS-CsChrimson* (C4da+epi). (B) Roll probability of larvae in response to two successive 40 mN mechanical stimuli spaced by the indicated amount of time (recovery duration). Genotype: *R38F11-GAL4/+*. (C) Roll probability of larvae expressing *UAS-TrpA1* in nociceptors exhibited levels of mechanically induced nociceptive potentiation comparable to other experimental genotypes used in the study (control*: UAS-TrpA1/+*; epidermis*: R38F11-GAL4, UAS-TrpA1/+*; nociceptors*: R27H06-GAL4, UAS-TrpA1/+*).

Figure 5. Epidermal cells are intrinsically mechanosensitive. (A) Schematic of preparation to measure radial stretch evoked calcium responses of dissociated epidermal cells. (B) Representative calcium responses of a dissociated epidermal cell to 0.5% and 1% radial stretch (successive stimuli), 2.5% radial stretch, and 5% radial stretch. (C) Dose response curve displaying the fraction of epidermal cells activated by increasing magnitudes of stretch. Red trace displays the mean ± SEM across six independent dissociated cell preparations, obtained from a minimum of 6 larvae. Gray traces display fraction responding in each dissociated cell preparation replicate. (D) Subsets of epidermal cells display varying stretch thresholds, n = 6 dissociated cell

preparations, for a total of 654 epidermal cells. (E) Representative mechanically induced epidermal calcium responses in the larval body wall. Images show GCaMP6s fluorescence intensity 100 ms prior to (i) and 20 s following (ii) a 25 μm membrane displacement (poke). (F) Distribution of the peak calcium response (F_{max}/F_0) to a 25 μm membrane displacement (poke) of 24 cells from 24 independent larval fillets. Cells were classified as responders (>10% increase in normalized GCaMP6s fluorescence). (G) Mean calcium responses (F/F_0) of poke responders and non-responders (n = 12 cells each). Solid lines depict mean normalized GCaMP6s fluorescence and shading indicates SEM. Genotype: *R38F11-GAL4, UAS-GCaMP6s*.

Figure 5 – figure supplement 1. Subsets of epidermal cells display calcium responses to diverse mechanical stimuli. Representative calcium traces of epidermal cells that respond to: (A) laminar flow via perfusion, (B) laminar flow and osmotic stretch, (C) 15% hypo-osmotic stretch, and (D) 30% hypo-osmotic stretch, or (E) do not respond to either flow or stretch. (F) Proportion of epidermal cells that are sensitive to mechanical stimuli. n = three distinct cell preparations, 6 larvae per preparation, for a total of 177 cells. (G) Related to Figure 5G. GCaMP6s responses (F/F_0) of individual epidermal cells to a 25 μm membrane displacement. Genotype: *R38F11-GAL4, UAS-GCaMP6s*.

Figure 6. CRAC channels are required for epidermal mechanosensory responses and epidermal nociceptive potentiation. (A) RNAi screen for epidermal ion channels required for mechanically induced nociceptive potentiation. Bars depict nociceptive potentiation index (difference in the larval roll probability to the first and second mechanical stimuli divided by roll probability to the first mechanical stimulus). Candidate channels were chosen for further analysis if they had a z-score greater than 2 (absolute value). (B) The CRAC channels Orai and Stim are required in epidermal cells for mechanically evoked nociceptive potentiation. Roll probability of larvae of the indicated genotypes (Control RNAi, *R38F11-GAL4, UAS-RFP-RNAi/+*; *Stim* RNAi, *R38F11-GAL4, UAS-Stim-RNAi/+*; *Orai* RNAi, *R38F11-GAL4, UAS-Orai-RNAi/+*) to a 40 mN mechanical stimulus followed by a second 40mN mechanical stimulus 10 s later. (C) *Drosophila* epidermal cells display classical store-operated calcium entry (SOCE). Treatment with the drug

thapsigargin (TG) in the absence of extracellular calcium promoted depletion of intracellular calcium stores and calcium influx, following extracellular calcium re-addition. (D) Like TG, 1% stretch in the absence of extracellular calcium induced depletion of intracellular calcium stores and calcium influx, following extracellular calcium re-entry. (E) 69% of stretch responsive cells displayed greater calcium influx during intracellular calcium stores release than during the calcium re-entry phase. (F-G) The Orai blocker, lanthanum chloride (500 nM) or the depletion of intracellular stores by thapsigargin (1 µM) reduces the fraction of stretch-sensitive epidermal cells. (H-I) The fraction of stretch-sensitive epidermal cells is significantly decreased in cells isolated from larvae expressing *Stim* RNAi, or *Orai* RNAi, as compared to control RNAi. (J) Stretch stimuli evoke dose-dependent calcium signals in the human keratinocyte HaCaT cell line. (K) Representative stretch evoked SOCE calcium response in HaCaT cells. Stretch induces calcium release from stores in the absence of extracellular calcium and a greater calcium influx in the presence of extracellular calcium. (L) Epidermal hyperpolarization enhances mechanical nocifensive responses. Roll probability of larvae expressing GtACR in epidermal cells (*R38F11-GAL4, UAS-GtACR/+*) or control larvae (*R38F11-GAL4/+*) to a single 70 mN mechanical stimulus. (M) Epidermal *Stim* overexpression enhances mechanical nocifensive responses. Roll probability of *Stim*-overexpressing larvae (*R38F11-GAL4, UAS-Stim/+*) and control larvae (*R38F11-GAL4/+*) to two successive 40 mN mechanical stimuli delivered 10 s apart. (N) Epidermal potentiation of mechanical nociceptive responses requires exocytosis. Roll probability of control larvae (*UAS-shi^{ts}/+*) or larvae expressing temperature-sensitive dominant-negative *shi* in epidermal cells (*R38F11-GAL4, UAS-shi^{ts}/+*) in response to two successive mechanical stimuli that followed 10 min of conditioning at the permissive (25º C) or non-permissive (30º C) temperature. (O) Model of epidermal-neuronal signaling. Mechanically evoked Stim/Orai calcium signaling in epidermal cells drives calcium influx and vesicle release that drives nociceptor activation and mechanical sensitization via activation of C4da nociceptors.

Figure 6 – figure supplement 1. Related to Figure 6A. Ion channel expression in epidermal cells. Five populations of *UAS-GFP*-expressing epidermal cells were selected

for RNA-seq analysis. GFP-positive epidermal cells were dissociated into single cell suspensions, manually picked, and subjected to RNA-Seq analysis. Plots depict expression levels (mean +/- standard deviation) of the indicated ion channels (log_2(TPM+1)) from n > 6 independent libraries for each sample type. (A) Expression in epidermal cells collected from *R38F11-GAL4* which labels all epidermal cells. (B) Anatomically defined subsets of epidermal cells were profiled by removing posterior segments from *R38F11-GAL4, UAS-GFP* larvae (*R38F11-GAL4* head and thorax) or (C) dissecting the ventral epidermis (*R38F11-GAL4* ventral epidermis). (D) Expression in the dorsal epidermis (*ush-GAL4*) and or (E) bands of epidermal cells (*R51F10-GAL4).*

Figure 6 – figure supplement 2. (A-B) Epidermal knockdown of ion channels affects larval mechanical nociceptive responses. Roll probability in response to the first and second mechanical stimulus for larvae expressing RNAi transgenes to (A) *Orai* or *attP40* RNAi control transgene and (B) *Task6* or *attP2* RNAi control transgene. (C) Epidermal cell SOCE is attenuated by pre-treatment with the Orai blocker, lanthanum chloride (100 nM). (D) Representative SOCE after treatment with TG (1 μm) in epidermal cells isolated from larvae treated with control RNAi, *Stim* RNAi (red), or *Orai* RNAi, (blue). (E) Peak calcium response following SOCE in epidermal cells isolated from larvae treated with control RNAi, *Stim* RNAi (red), or *Orai* RNAi, (blue). (F) *Stim* RNAi decreases calcium store content of epidermal cells. Calcium store content was measured as the area under the curve of the cytosolic calcium response to TG (1 μm) in the absence of extracellular calcium.

Supplementary File 1. Details of statistical analyses performed for this study, including comparison groups, statistical tests, and results.

Figure 1

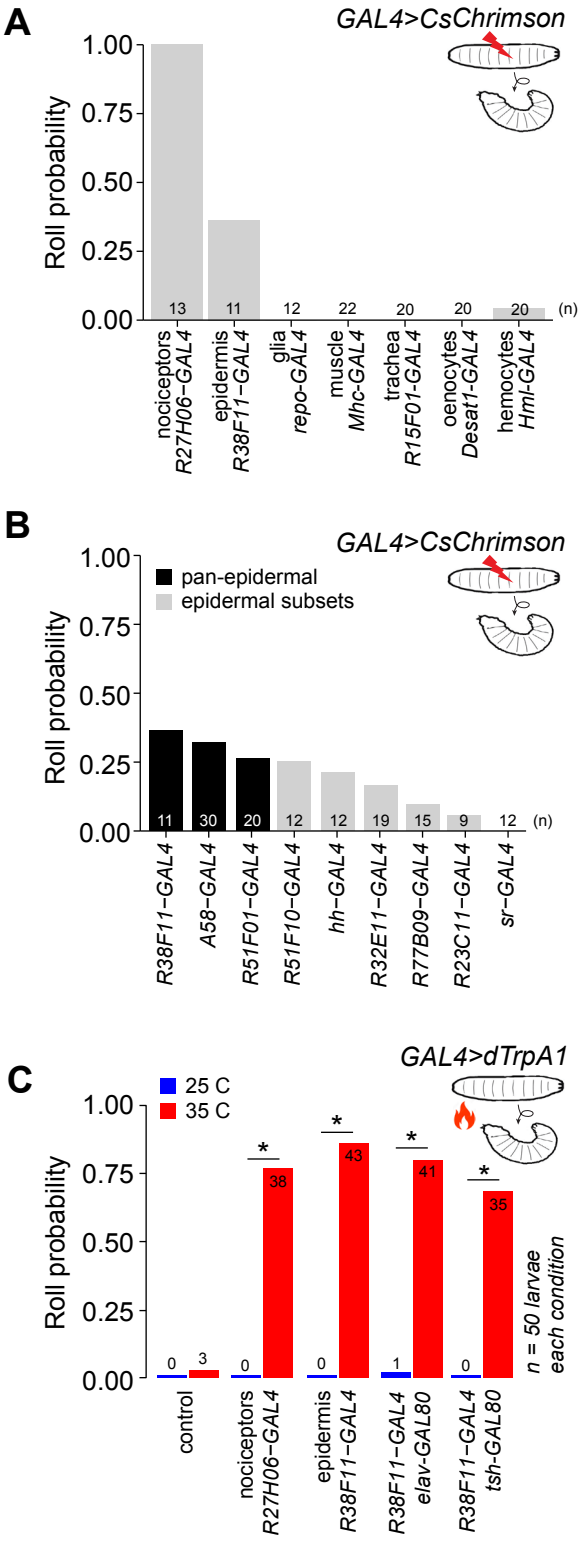

Figure 2

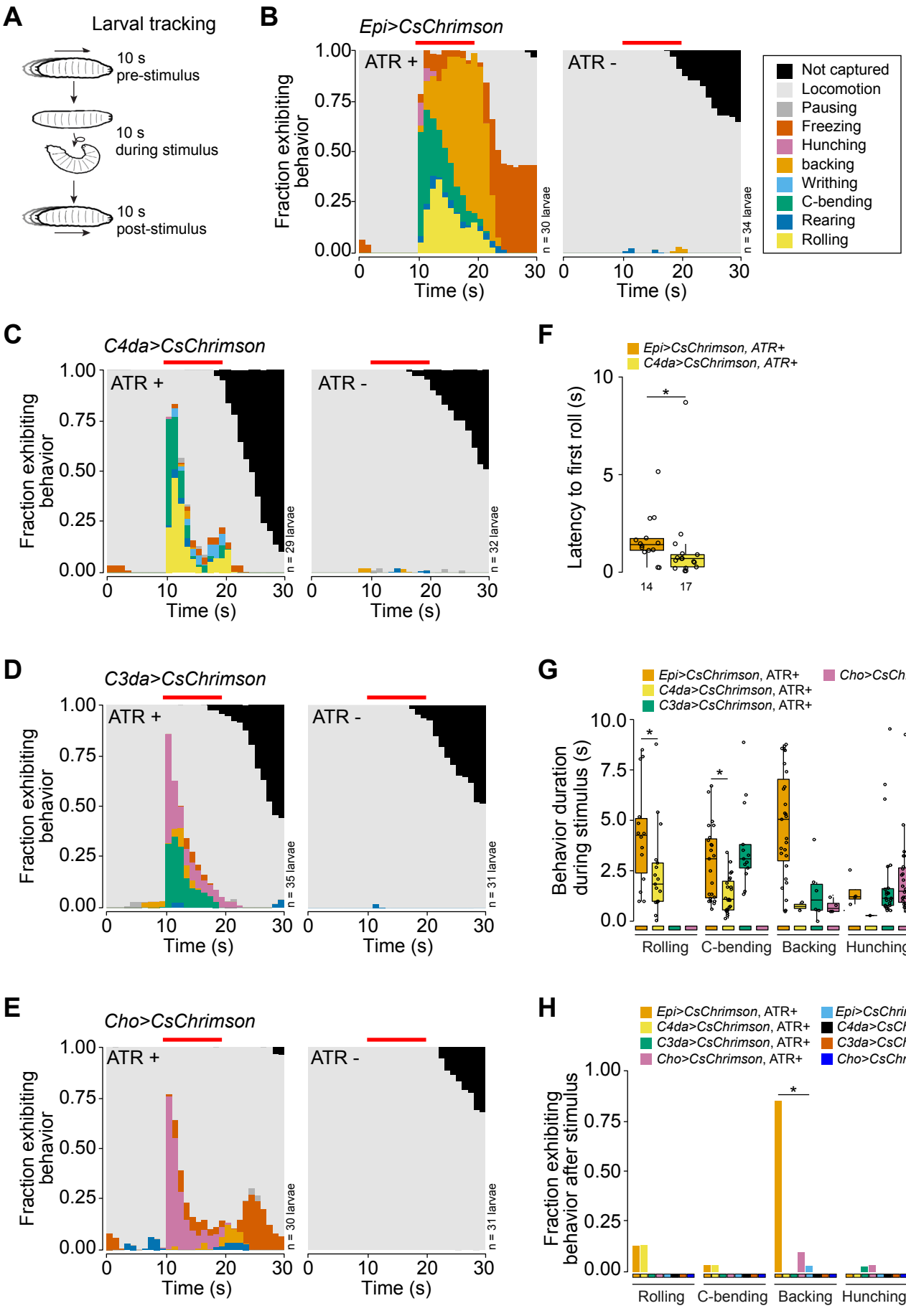

Figure 3

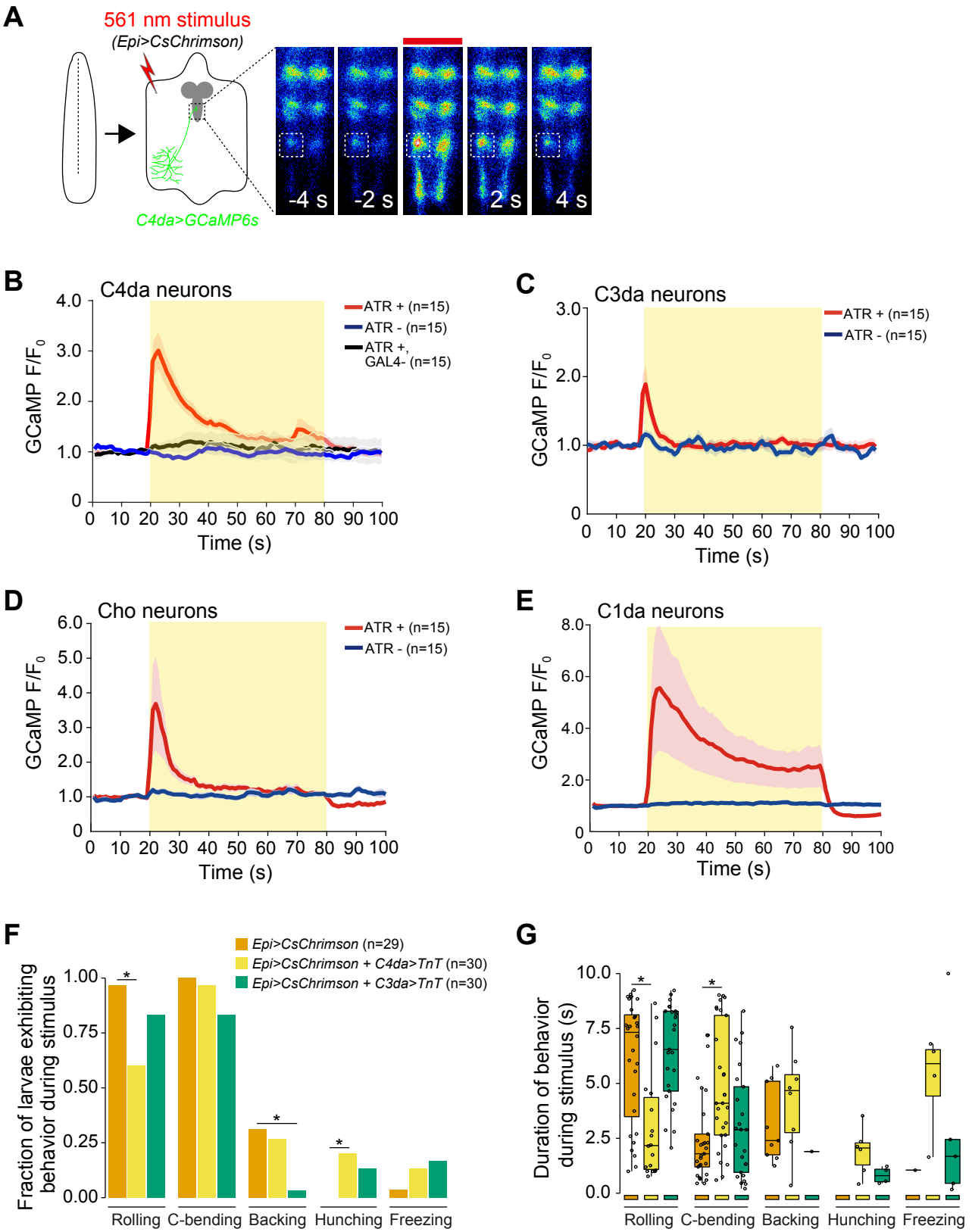

Figure 4

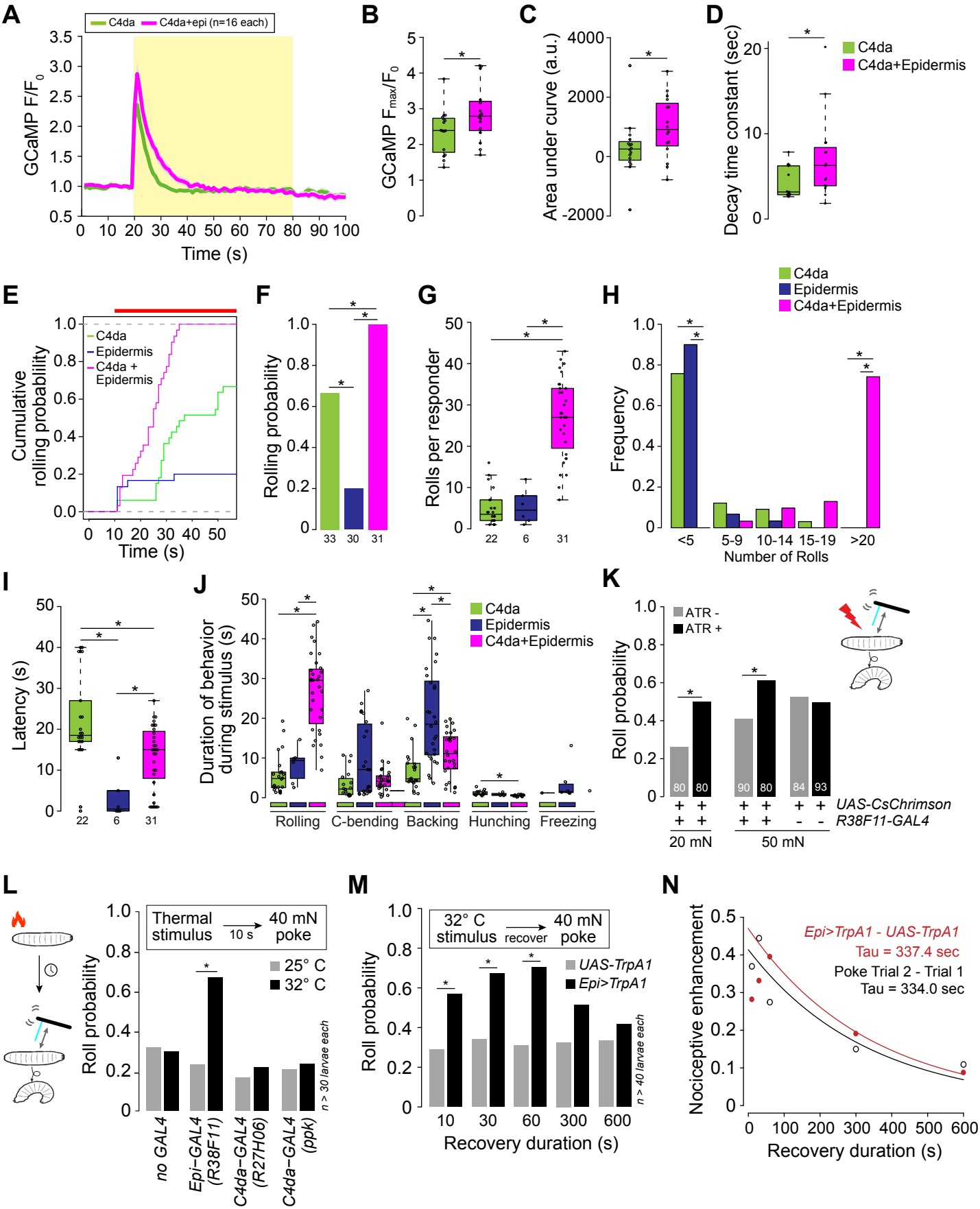

Figure 5

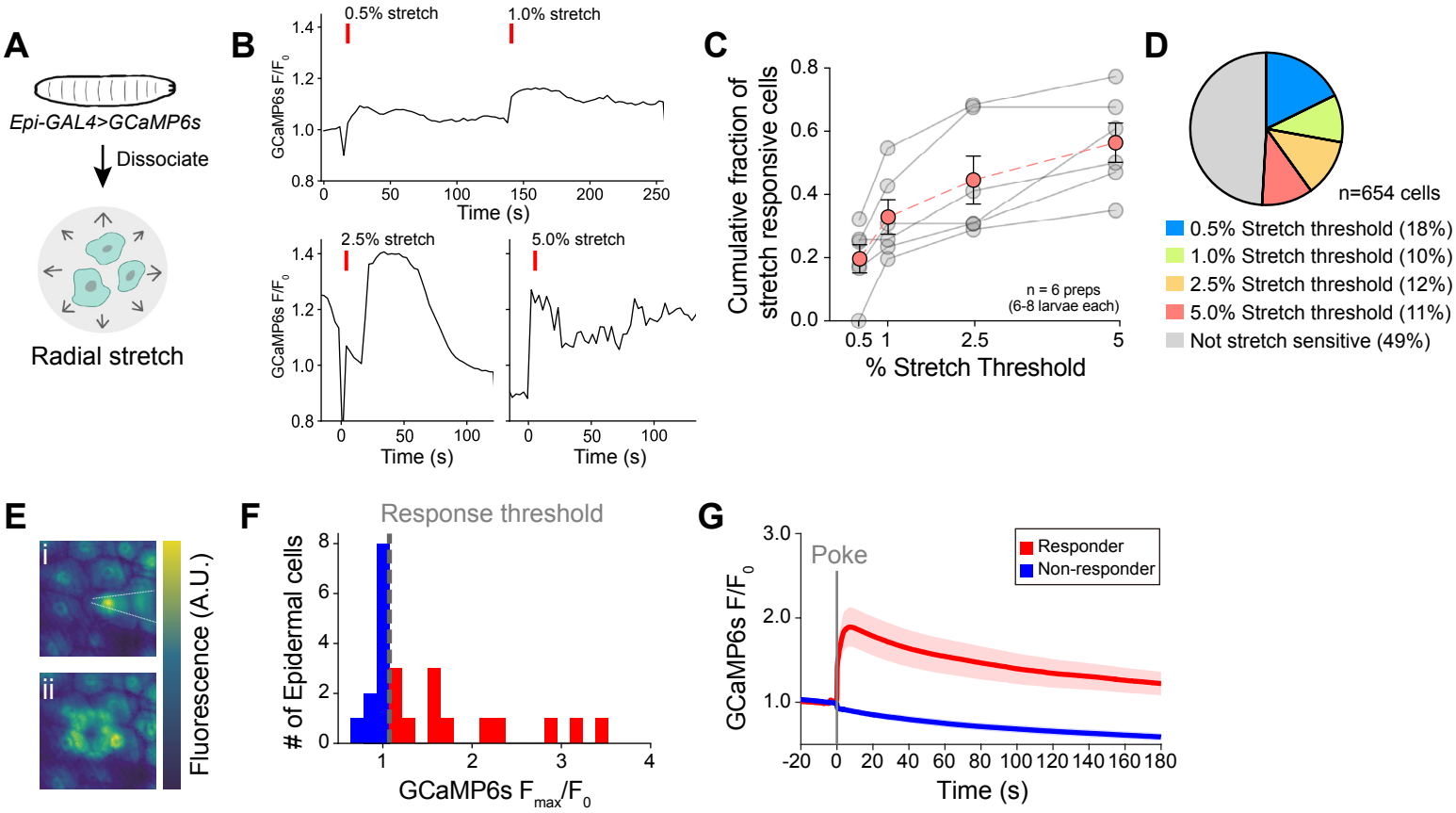

Figure 6